

RESEARCH ARTICLE

Stem Cells, Tissue Engineering, Development, and Cancer

Human placental-derived stem cell therapy ameliorates experimental necrotizing enterocolitis

Victoria G. Weis,¹ Anna C. Deal,¹ Gehad Mekkey,^{1,2} Cara Clouse,¹ Michaela Gaffley,^{1,3} Emily Whitaker,¹ Cole B. Peeler,^{1,4} Jared A. Weis,^{4,5,6} Marshall Z. Schwartz,¹ and Anthony Atala¹

¹Wake Forest Institute for Regenerative Medicine, Winston-Salem, North Carolina; ²Faculty of Science, Zagazig University, Zagazig, Egypt; ³General Surgery, Wake Forest School of Medicine, Winston-Salem, North Carolina; ⁴School of Biomedical Engineering and Sciences, Virginia Tech-Wake Forest University, Blacksburg, Virginia; ⁵Department of Biomedical Engineering, Wake Forest School of Medicine, Winston-Salem, North Carolina; and ⁶Comprehensive Cancer Center, Wake Forest Baptist Medical Center, Winston-Salem, North Carolina

Abstract

Necrotizing enterocolitis (NEC), a life-threatening intestinal disease, is becoming a larger proportionate cause of morbidity and mortality in premature infants. To date, therapeutic options remain elusive. Based on recent cell therapy studies, we investigated the effect of a human placental-derived stem cell (hPSC) therapy on intestinal damage in an experimental NEC rat pup model. NEC was induced in newborn Sprague-Dawley rat pups for 4 days via formula feeding, hypoxia, and LPS. NEC pups received intraperitoneal (ip) injections of either saline or hPSC (NEC-hPSC) at 32 and 56 h into NEC induction. At 4 days, intestinal macroscopic and histological damage, epithelial cell composition, and inflammatory marker expression of the ileum were assessed. Breastfed (BF) littermates were used as controls. NEC pups developed significant bowel dilation and fragility in the ileum. Further, NEC induced loss of normal villi-crypt morphology, disruption of epithelial proliferation and apoptosis, and loss of critical progenitor/stem cell and Paneth cell populations in the crypt. hPSC treatment improved macroscopic intestinal health with reduced ileal dilation and fragility. Histologically, hPSC administration had a significant reparative effect on the villi-crypt morphology and epithelium. In addition to a trend of decreased inflammatory marker expression, hPSC-NEC pups had increased epithelial proliferation and decreased apoptosis when compared with NEC littermates. Further, the intestinal stem cell and crypt niche that include Paneth cells, SOX9+ cells, and LGR5+ stem cells were restored with hPSC therapy. Together, these data demonstrate hPSC can promote epithelial healing of NEC intestinal damage.

NEW & NOTEWORTHY These studies demonstrate a human placental-derived stem cell (hPSC) therapeutic strategy for necrotizing enterocolitis (NEC). In an experimental model of NEC, hPSC administration improved macroscopic intestinal health, ameliorated epithelial morphology, and supported the intestinal stem cell niche. Our data suggest that hPSC are a potential therapeutic approach to attenuate established intestinal NEC damage. Further, we show hPSC are a novel research tool that can be utilized to elucidate critical neonatal repair mechanisms to overcome NEC.

ileum; LGR5 + stem cell; necrotizing enterocolitis; neonatal; stem cell therapy

INTRODUCTION

Necrotizing enterocolitis (NEC) is a life-threatening intestinal disease in premature infants. Correlating with the degree of prematurity, NEC affects 5%–10% of premature infants and continues to be a leading cause mortality in premature infants (1, 2). Decades of research have shown NEC is a multifaceted disease that results from the complex interaction of early bacterial colonization, an exaggerated inflammatory response, and immature intestinal epithelium. The premature intestine with an immature immune system can

become hyperinflammatory in response to early bacterial colonization (3). In human and animal studies, NEC pathogenesis is accompanied by a significant influx of pathogenic immune cells and increased inflammatory cytokine signaling (4–7). Early bacterial colonization can also directly damage the epithelial barrier of the intestine. Uniquely upregulated in the premature intestinal epithelium, Toll-like receptor 4 (TLR4), a recognition receptor for Gram-negative bacterial endotoxin LPS, is a key initiator of NEC pathogenesis (8). Bacterial LPS activates TLR4 in the premature epithelium and triggers increased enterocyte cell death coupled





with decreased proliferation of intestinal stem cells that results in the loss of a stable epithelial barrier (9). Additionally, Paneth cells located in the crypts serve a central role in supporting intestinal stem cell niche homeostasis and protecting against pathogens (10, 11). As recent studies have shown, loss of Paneth cells can also contribute to NEC pathogenesis (12-14). Together, these epithelial effects lead to barrier dysfunction and impaired regeneration. The neonatal repair processes are not able to counter the cyclic damage of bacterial translocation, uncontrolled inflammation, and epithelial damage. In this milieu, NEC pathologies can develop including feeding intolerances, bloody stool, and distended and necrotic intestine, eventually lead to systemic sepsis. Although our understanding of instigating factors and protective strategies continues to advance, treatment options for established NEC disease have remained relatively unchanged.

As known instigating factors, the microbiome, immune response, and epithelial development have been the focus of preventative and therapeutic investigations in NEC disease. Breast milk has been shown to protect against NEC-instigating pathways and reduce NEC incidence in experimental NEC models and in premature infants (15-17). Recently, amniotic fluid has demonstrated similar affects experimentally (18). Accordingly, these fluids contain bioactive factors that inhibit TLR4-mediated epithelial injury, reduce inflammatory signaling integral to NEC pathogenesis, and support intestinal maturation (15, 18). Similarly, probiotic administration has vielded promising results in establishing a healthy microbiome, supporting epithelial development, and reducing NEC incidence (19, 20). These protective pathways have led to new potential prophylactic strategies to reduce the risk of NEC onset. However, they alone often fail to resolve already established NEC damage and therefore are currently limited to the prevention of onset (21). Currently, no effective treatments that can heal established NEC disease are available.

Emerging perinatal stem cell approaches from our group and others have been shown to possess dual supporting roles in modulating pathogenic inflammation and resolving epithelial damage through multiple regenerative pathways (22-25). In experimental NEC, perinatal stem cells can decrease inflammatory signaling, improve epithelial function, and reduce NEC damage (25-27). As few of the perinatal stem cells were observed to engraft into the intestine in these studies, the beneficial effects were exerted predominantly via paracrine signaling (25). Further, perinatal stem cell conditioned media or exosomes via various administration routes can reduce NEC damage and mortality in experimental NEC (25, 28). Previous perinatal cell studies have focused on stem cells derived from amnion or amniotic fluid obtained mostly via amniocentesis procedures. However, the placenta, long considered medical waste that can simply be collected after healthy birth, is now being regarded as a more optimal tissue for perinatal stem cell isolation. hPSC possess similar proliferative and multipotency characteristics to other perinatal stem cells; however, they also express a unique secretome (29). hPSC have been shown to have immunomodulatory factors and capabilities (30) and also express several factors that can directly promote intestinal epithelial healing and regeneration, including ICAM1, NRG1, EGFR, and lactoferrin (29). Together, these data suggest that hPSC may be a potential multifaceted therapy to combat NEC pathogenesis.

In this study, we hypothesized that hPSC administration after the onset of NEC induction would ameliorate the intestinal damage in an experimental model of NEC through immunomodulation and attenuation of epithelial disruption. Expanding upon previous NEC neonate rat models that show NEC damage starting at 24 h (31-33), we increased the LPS doses during the first 30 h of NEC induction to allow the disease to progress further before the first hPSC injection. This adjusted timetable allows for more precise investigation of hPSC for therapeutic versus prophylactic use. Additionally, we designed our NEC model to yield a highly reproducible and narrowly staged disease to closely align with the earlier stages of human NEC (Modified Bell's Stages I and II). This focused disease range of suspected NEC and mild NEC staging allows us to specifically study potential hPSC therapy as an early intervention in medically managed NEC. Here, we evaluated the efficacy of hPSC treatment on survival, clinical symptoms, gross intestinal health, and cellular ileal damage including inflammatory signaling and epithelial cell composition. Using our modified NEC model, our results show that hPSC treatment can promote intestinal healing of NEC damage, in part by restoration of the intestinal stem cell niche. These findings also have important implications in providing a pivotal research tool that can be leveraged to identify reparative mechanisms and potential targets in combating NEC disease.

MATERIALS AND METHODS

Placental Cell Isolation, Expansion, and Culture

Consent for obtaining human placenta was obtained from patients before giving birth with adherence to the protocol approved by the Institutional Review Board of Wake Forest University. The Manufacturing Development Center within the Wake Forest Institute for Regenerative Medicine (WFIRM), Wake Forest School of Medicine, collected the full-term placenta specimens. From the whole placental tissue, the chorion was biopsied and then digested to isolate perinatal placental cells as previously described (29, 34). Briefly, isolated placental cells were plated in α-MEM supplemented with AmnioMax and Glutamax. After cell expansion, cell selection for C-kit positive cells was performed with a CD117 antibody (Cat No. 120-099-672, Miltenyi Biotec, Germany) in a Miltenyi Mini Macs System. Selected C-kit positive placental cells (hPSC) were expanded in culture and underwent sterility, endotoxin, mycoplasma, and Karyotype testing. Further, phenotypic testing of placental cell cultures confirmed CD29(+), CD44 (+), CD73(+), CD105(+), CD146(+), SSEA-4(+), HLA-ABC (+), CD34(-), CD45(-), and HLA-DR(-). Cells were cryopreserved in CryoStor10 until further use. For NEC studies, hPSC between passage 8 and 12 were cultured to no more than 70% confluency. hPSC were harvested, washed twice with DPBS, and diluted to 2×10^6 cells per 50 μL in DPBS for injection.

NEC Animal Model

The care, maintenance, and treatment of animals in these studies adhere to the protocols approved by the Institutional

Animal Care and Use Committee of Wake Forest University. Timed-pregnant Sprague-Dawley rats were obtained from Charles River Laboratories and monitored for birth beginning 36h before expected birth. Within 6h of birth, both male and female newborn pups from each litter were randomly divided into three groups: breastfed (BF) controls (n =11), NEC (n = 11), and NEC with subsequent hPSC therapy (NEC-hPSC, n = 11). Following randomization, sex of pups was not considered a biological variable in further analysis. BF controls were left with dam and received no additional stressors. NEC pups were separated from dam and housed in a Caleo Infant Incubator (Drager, PA) at 30°C with 50% humidity for the remainder of the study. NEC was induced with modifications of an established protocol (21, 25, 33, 35). NEC pups were oral gavage fed via a 22ga plastic feeding tube (Instech Laboratories, PA) 4× per day with a hyperosmolar formula prepared from 15 g Similac PM 60/40 (Abbott Nutrition, OH) in 75 mL Esbilac canine supplement (Pet-Ag, IL). NEC pups also received oral administration of LPS (Cat no. L3012, Sigma, MO; $4 \mu g/g$, $3 \times$ within 30 h of birth), and hypoxia (5% O_2 for 10 min, $3\times/day$) (Fig. 1). NEC pups each received two doses of either 50 μ L DPBS (NEC group) or 2 \times 10⁶ hPSC in DPBS via intraperitoneal (ip) injection. Timed for after initial NEC damage onset (31-33), the first hPSC injection was given after the last of the three LPS doses (32 h of NEC induction) with a second hPSC injection 24h later (56 h). A subset of pups also received an intraperitoneal injection of EdU (50 mg/kg, Cayman Chemical, MI) 24 h before euthanasia. To avoid previously observed fluid leakage from the injection site, all injections were performed under light anesthesia with pups receiving similar doses and lengths of anesthesia (<10 min of Isoflurane). At 96 h of NEC induction, all remaining pups were euthanized.

Placental Cell Localization

hPSC localization was first examined in an exploratory pilot cohort of 5 NEC-hPSC pups using dual-labeled hPSC for in vivo cell tracking and immunohistochemical analysis. As previously shown (36), hPSC were dual-tagged via lentiviral infection with a luciferase from Renilla reniformis (renLUC, for in vivo cell tracking) and mKATE (for IHC). NEC-hPSC pups received dual-labeled hPSC (referred to as mKATE hPSC) for the first cell injection (at 32h) followed by untagged hPSC in the second cell injection. For in vivo imaging on day 4, the luciferase substrate (Colenterazine 200 µg/kg) was intraperitoneally injected and in vivo imaging system (IVIS) images were obtained 5 min after substrate injection (36). An untreated NEC pup was used as an imaging control. For immunohistochemistry, the intestinal tissue was processed as described in Immunostaining and Quantifications and immunostained with a rabbit polyclonal anti-tRFP antibody that recognized mKATE (Cat No. AB233, Evrogen, NY) (36).

To detect hPSC engraftment in all 11 NEC-hPSC pups in our study, PCR for the presence of the human GUS gene was used. As previously shown (37), the rat GUS gene is not detected by the primers used for human GUS (hGUS forward: 5'-AGT GTT CCC TGC TAG AAT AGA TGA-3', reverse: 5'-AAA CAG CCT GTT TAC TTG AGC A-3'). First, DNA was isolated from a small biopsy of frozen distal ileum using a DNeasy Blood and Tissue kit (Qiagen, MD) according to the manufacturer's instructions. Equal amounts of gDNA (200 µg) were analyzed by PCR with Qiagen Fast Cycling PCR kit (40 cycles). Used as a loading control, PCR for GAPDH was performed with primers that detect both the human and rat GAPDH gene (GAPDH forward: 5'-ACC ACA GTC CAT GCC ATC AC-3', reverse: 5'-TCC ACC ACC CTG TTG CTG

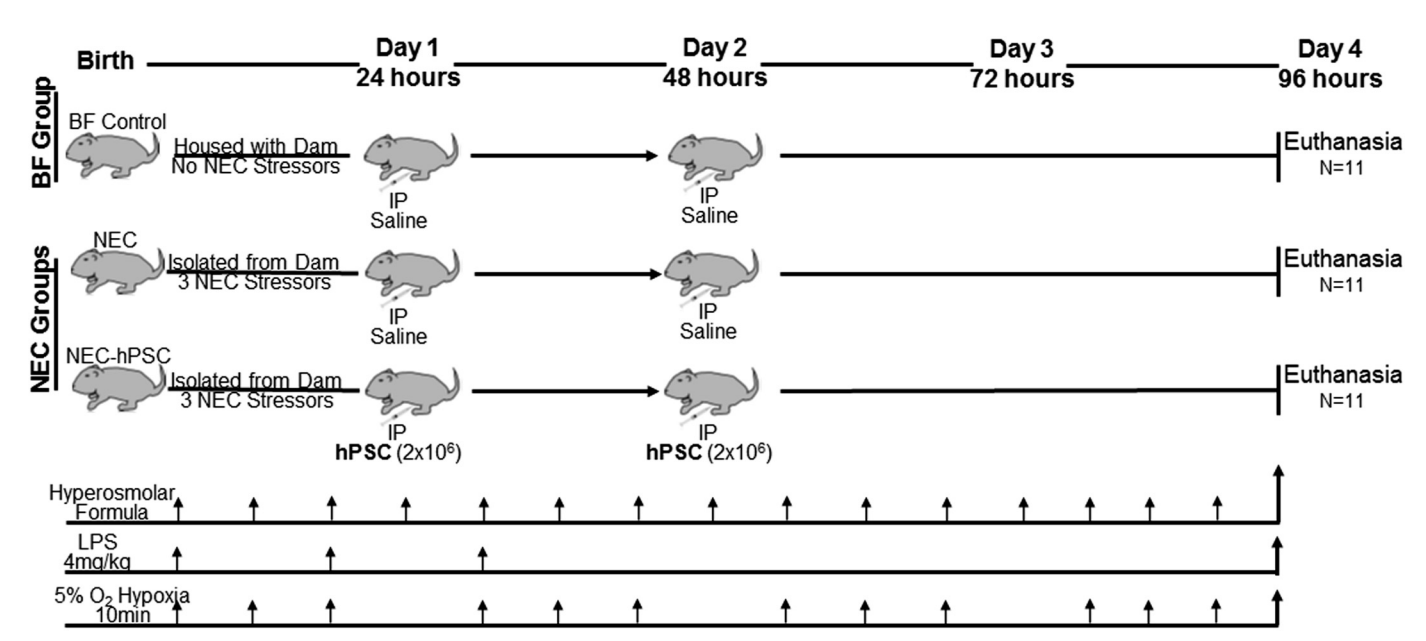


Figure 1. Study design schematic. Newborn Sprague-Dawley rats (male and female) were randomly divided into three groups: BF control, NEC, and NEC-hPSC. Within 6 h of birth, NEC and NEC-hPSC pups began receiving the three NEC stressors of hyperosmolar formula feeding, LPS oral dosing, and whole animal hypoxic stress. After administration of the three LPS doses, NEC pups received an initial intraperitoneal injection of saline (NEC) or hPSC (NEC-hPSC) at 32 h with a second intraperitoneal injection 24h later. Body weight and Clinical Sickness Score were assessed daily. All remaining pups were euthanized at 96 h resulting in n=11 for all experimental groups. BF, breastfed; hPSC, human placental-derived stem cell; NEC, necrotizing enterocolitis.



TA-3'). BF ileum and mKATE hPSC were used as a negative and positive controls, respectively.

Survival, Weight, and Clinical Sickness Score

Pup death or humane euthanasia up to the 96-h endpoint was assessed. Pup deaths caused by known or suspected adverse technical events (perforation, formula aspiration) were removed from the survival analysis (n = 2). Body weight and a Clinical Sickness Score were assessed at birth and every 24 h. Because of variations in birth weights of litters, weight was analyzed as the daily change in weight to minimize litter to litter variations. The previously reported Clinical Sickness Score (25, 33) is a composite score of four criteria: appearance, response to touch, natural activity, and body color.

Macroscopic Score and NEC Grade

Following euthanasia, the entire intestine (duodenumcolon) was excised with removal of its surrounding and connective tissues, straightened, and photographed. A Macroscopic Score was assessed based on consistency/fragility, color, and degree of dilatation as previously described (25, 33). Extent of dilation and severity was further assessed by a custom-built software that allows measurement of diameter along the length of the intestine. Images were processed by semiautomatic segmentation and image morphological operations to yield a region-of-interest (ROI) mask of the intestine using an active contour-based region growing algorithm (38) to automatically refine a manually designated initial ROI. The final segmentation of each intestine was then manually reviewed and edited, if necessary, to ensure optimal segmentation. Next, the diameter along the length of the intestine was calculated using a Euclidean distance transform of the masked ROI. Distances were calibrated using a reference scale that was photographed within the same image field as the intestine. The medial ileal diameter for each animal was then calculated using diameter measurements in 100-μm increments along the length of the ileum with the ileum designated as the final third of the total intestinal length. To determine the extent of pathological involvement of the ileum, the median ileal diameter in the BF group was used as the healthy dilation control. Pathological distention was then defined as an ileal diameter (within the 100-um increment) greater than the BF median diameter plus 2 standard deviations. The percentage of pathological involvement for each animal was calculated by determining the length of the ileum defined as pathologically distended divided by the total length of the ileum.

For histological assessment, the small intestine was fixed in 4% paraformaldehyde overnight at 4°C and embedded in paraffin. The full length of the intestine was placed in a zigzag pattern and embedded on same plane at the bottom of the cassette. When sectioned, each section includes a 4-um thick slice along the entire length of the intestine from duodenum to ileum. This all allows for histological examination and analysis along the entire length of the ileum (designated as the final third of the total small intestinal length). Sections were deparaffinized, rehydrated, and hematoxylin and eosin (H&E) staining was performed. Based on a previously established scoring system to assess NEC damage (25, 33), H&E-stained sections that included the full ileal length was evaluated for an overall NEC Grade: 0 (normal), 1 (disarrangement of villus cells, mild villus core separation), 2 (disarrangement of villus cells, severe villus core separation), 3 (epithelial sloughing), and 4 (bowel necrosis/perforation). NEC was defined as grade 2 or above. The H&E sections were then imaged at ×10 with an EVOS FL Auto 2 Cell Imaging System (Invitrogen, CA) to measure extent of ileal involvement of each NEC Grade along an average total length of 2-3 cm of ileum. For this, the linear length of ileum with each NEC Grade was measured and then normalized by the total linear length of the ileum (% involved = length_{Grade}/total ileal length).

qPCR Analysis

To examine inflammatory signaling, a small section of distal ileum was frozen for RNA isolation. RNA was extracted with TRIzol (Invitrogen) according to the manufacturer's instructions. The RNA (1µg) was treated with RQ1 RNasefree DNase (Promega, WI) and then reverse-transcribed using High-Capacity cDNA RT kit (Applied Biosystems, CA). Equal amounts of each cDNA were analyzed by real-time PCR with specific primers and PowerUp SYBR Green (Invitrogen) in an ABI QuantiStudio 3 real-time PCR system. Each sample was measured in triplicate. The following predesigned primers from IDTDNA (CA) were used: TNFa forward: 5'-GTC TTT GAG ATC CAT GCC ATT G-3', reverse: 5'-AGA CCC TCA CAC TCA GAT CA-3'; IL-1\beta forward: 5'-TTG TCG TTG CTT GTC TCT CC-3', reverse: 5'-GTG CTG TCT GAC CCA TGT-3'; NFκB forward: 5'-GAC TCT TCT TCA TGA TGC TCT TG-3', reverse: 5'-GAG TTC CAG TAC TTG CCA GAC-3'; and TBP forward: 5'-GGA GAA CAA TTC TGG GTT TGA TC-3', reverse: 5'-TGT GAA GTT CCC CAT AAG GC-3'. As previously described (39), cycle threshold was converted to relative expression via the $2^{-\Delta\Delta}$ cycle threshold method, using TATA-box-binding protein (TBP) as an endogenous control. The mean value of the normalized cycle thresholds of all breastfeed rat samples was used as a reference.

Immunostaining and Quantifications

Paraffin sections were deparaffinized and rehydrated before antigen retrieval was performed using Antigen Retrieval Buffer (Abcam, MA) in a pressure cooker for 15 min. After cool-down on ice, sections were blocked with protein block serum free (Dako, Denmark) for 1h at room temperature. The following primary antibodies were incubated at 4°C overnight: Rabbit anti-Cleaved Caspase 3 (Cat No. 9661, Cell Signaling Technologies, MA), Rabbit anti-OLFM4 (Cat No. 39141T, Cell Signaling Technologies), Mouse IgG_{2b} anti-Ezrin (Cat No. CPTC-Ezrin-1, Developmental Studies Hybridoma Bank, IA), Rabbit anti-Lysozyme (Cat No. MBS2556232, MyBioSource, CA), Rabbit anti-SOX9 (Cat No. AB5535, Sigma, St. Louis, MO), and Rabbit anti-β-catenin (Cat No. 51067-2-AP, Proteintech, IL). After three washes in 1× phosphate-buffered saline for 5 min each, sections were incubated for 1h at room temperature with the appropriate secondary antibodies conjugated for immunofluorescence with Alexa Fluor 488, Cy3, or Cy5 (1:1,000; Jackson ImmunoResearch, PA). Slides were then washed and incubated with 4',6-diamidino-2-phenylindole (DAPI; 1:10,000) for 5 min. After additional washing, slides were mounted with ProLong Gold Antifade Reagent (Invitrogen). For EdU detection, Click-iT EdU Proliferation kit for Imaging was used (Invitrogen). Briefly, after antigen retrieval, slides were blocked with 3% BSA, permeabilized with 0.5% Triton X-100, and EdU labeled followed the manufacturer protocol. Coimmunostaining then proceeded to protein block as described above. Sections were imaged using an Olympus FV3000 fluorescent microscope (Olympus) equipped with a Nuance EX camera (PerkinElmer) or EVOS FL Auto 2 Cell Imaging System (Invitrogen).

Ezrin immunostaining (with phase contrast as needed) was used for villus/crypt height quantification. From each animal, three images were taken of randomly selected regions of the ileum. Well-oriented crypts and villi were identified in each $\times 20$ field image and the height of each was measured using FIJI. The villi were measured from the villus tip to the crypt transition, and the crypts were measured from the crypt transition to the bottom of the invagination between two villi. Cleaved caspase 3, EdU, OLFM4, Ezrin, SOX9, and β-catenin immunostainings were quantified from three randomly selected ×20 field images (equally ~1 to 1.5-mm length of the ileum) from each animal as previously described (40). Briefly, positively stained cells within the epithelial layer, the top of villi, and the base of crypts were manually marked in individual "layers" using Photoshop (Adobe Systems, CA). Analysis of total positive cell numbers and quantitative spatial localization along the crypt-villi axis was conducted with a modified custombuilt MATLAB software (Mathworks, MA) previously described (40). Total cell counts were normalized to the linear length of ileal tissue quantified as automatically measured from the "crypt base" contour line (with an average of 1-1.5 mm of ileum). Histograms with bin widths equal to 25 pixels (10 μm) were generated for each marker expression along the cryptvillus axis. Cell counts in histogram bins were normalized to the total number of crypts manually counted in each animal to reflect the average number of cells per crypt that are localized within each bin location. Histograms are reported as a mean histogram line with standard deviation designated as a shaded region. Similar total cell counts and distributions were found between normalization to crypt number and the linear length assessed. As Paneth cells are not as abundant in 4-day-old rat pups, larger regions of lysozyme-immunostained ileal sections (4-8 mm for each animal) were scanned with an EVOS system (Invitrogen), and the total number of lysozyme⁺ epithelial cells per linear ileal length assessed was manually quantified using FIJI. Although initial investigation showed minimal differences in the number of crypts per millimeter, the ileal length in the three selected images was chosen for normalization of the total cell counts to minimize any potential difficulties in crypt identification in NEC-damaged tissue and therefore allow for more high-throughput analysis.

Statistical Analysis

The change in body weight and clinical sickness score data was analyzed by fitting a mixed model as implemented in GraphPad Prism 8.0. This mixed model uses a compound symmetry covariance matrix and is fit using restricted maximum likelihood. The Geissner-Greenhouse correction was used to correct for violations of the sphericity assumption. In the presence of missing values, the results from this

mixed model can be interpreted like a repeated measures two-way ANOVA (with Time and Score/Weight Change as the two factors). Statistical significance (P < 0.05) between groups at each time point was determined with post hoc tests using Fisher LSD and controlling the false discovery rate (5%) (Benjamini and Hochberg) to correct for multiple corrections. Within each experimental group, significance between each day (i.e., DO vs. D1) was also assessed and listed in Supplemental Table S1 (all Supplemental material is available at https://doi.org/10.6084/m9.figshare.13070420). For all end point measurements (Macroscopic Scores, NEC Grade, qPCR, and IHC quantification), a Kruskal-Wallis test was first performed to determine whether there were statistically significant differences between the three groups (statistical significance set at P < 0.05). A significant Kruskal–Wallis test was then followed by post hoc Conover test with Holm familywise error rate correction to determine which groups were statistically different (BF vs. NEC, NEC vs. NEC-hPSC, and BF vs. NEC-hPSC). Statistical significance set at P < 0.05. The P values for all comparisons and statistical tests conducted in this study are included in Supplemental Table S1.

RESULTS

The NEC animal model was successfully replicated with increasing insult before treatment and decreased survival in all experimental groups. Beginning within 6 h of birth, neonatal rat NEC models utilize formula feeding, LPS administration, and hypoxic stress to induce NEC (33). Previous investigations have established that intestinal damage is initiated within 24 h of NEC induction, while overall mortality limits the study window to 96 h (31-33, 41). To increase intestinal insult before our treatment time point, the NEC rat pup model used in the present study included three doses of LPS within the first 30 h of NEC induction (Fig. 1) in comparison to one to two LPS doses of previous experimental NEC studies (25, 27, 33). Accordingly, pups undergoing NEC stressors showed body weight loss and increased Clinical Sickness Scores within 24 h and these symptoms continued to worsen until the 96-h end point (Fig. 2, A and B). Breastfed (BF) controls gained weight from birth to end point and showed no significant clinical symptoms for the duration of the study.

To study hPSC therapeutic potential, two injections of 2 \times 10° hPSC were given 24 h apart following completion of LPS administration (Fig. 1). These injection time points strategically occurred after the previously reported intestinal damage initiation at 24h and the observed onset of clinical symptoms in the present study (Fig. 2, A and B). Prior to hPSC administration, NEC-hPSC pups and untreated NEC pups showed similar body weight loss and increased Clinical Sickness Scores. After the second hPSC injection, body weight loss and Clinical Sickness Scores began trending toward improvement in NEC-hPSC pups; however, these trends did not reach statistical significance by the 96-h end point (Fig. 2, A and B). No difference between the groups was observed in survival at day 4 (Fig. 2C).

hPSC Treatment Improved Gross Intestinal Pathology

As NEC pathologies are predominantly found in the distal small intestine, we focused our analysis on the ileum in our

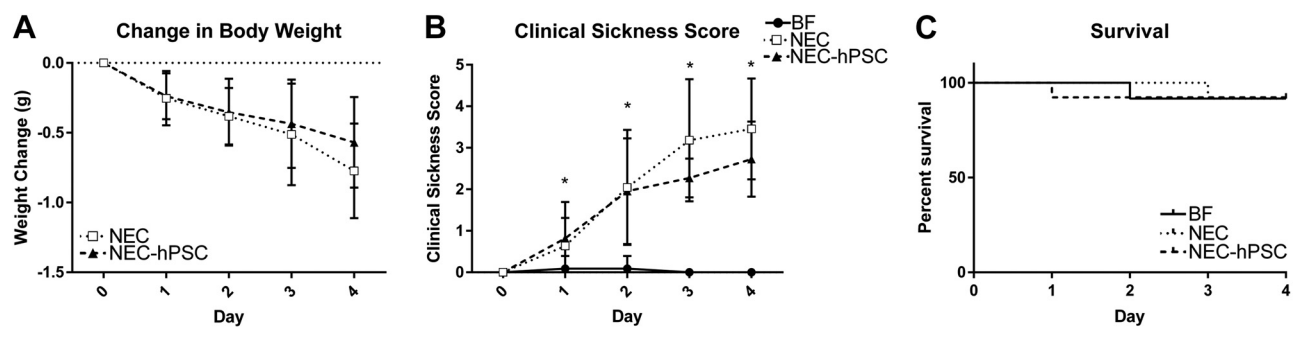


Figure 2. Whole animal assessments of mortality and symptoms. A: NEC and NEC-hPSC animals had noticeable weight loss beginning within 24 h before initial intraperitoneal injections. Both groups continued to lose weight until study conclusion. While NEC-hPSC animals appeared to trend toward slower weight loss in the last 48 h, a statistical difference was not reached between weight loss changes of the two groups. B: a composite score called Clinical Sickness Score was used to assess clinical symptoms and overall health of the animal (0 = healthy, normal). BF animals show no clinical symptoms. NEC and NEC-hPSC animals have increased symptoms by day 1 (24 h) compared with BF controls (*P < 0.03). The Clinical Sickness Scores of NEC and NEC-hPSC animals are identical until day 2 when NEC-hPSC scores begin trending lower. However, no statistical difference is observed at the study endpoint of 96 h. C: no significant difference was observed in survival. Overall, each group lost one animal over the course of the 4-day study. Mean values with standard deviation are plotted (n = 11 for each group). Statistical comparison by a mixed model analysis corrected for multiple comparisons with Fisher's Least Significant Difference (LSD) method are available in Supplemental Table S1. The animals lost prior to the 96-h endpoint were not included in further analyses. BF, breastfed; hPSC, human placental-derived stem cell; NEC, necrotizing enterocolitis.

studies. Upon gross ileal examination in NEC pups, obvious pathologies of dilation and tissue fragility were observed (Fig. 3 and Supplemental Fig. S1). A previously established composite score for dilation, coloration, and consistency/fragility (33) was used to assess the gross pathological symptoms on a scale of 0-2 (Fig. 3B). The NEC induction procedures increased the ileal "Macroscopic Score" in NEC pups compared with BF controls (NEC: 1.18; BF: 0.06). However, NEC pups treated with hPSC had a significantly reduced gross pathology composite score compared with untreated NEC ileum (NEC-hPSC: 0.76). While all three of the individual score components contributed in part to the increased score in NEC pups, consistency and dilation were the score-driving factors for the reduced pathology in NEChSPC pups (Supplemental Fig. S1, A-C).

We sought to further investigate the severity and tissue burden of the ileal dilation. A custom software was developed to automate measurements of the exact ileal diameter along the length of the tissue. This method allowed for a quantitative analysis of the intestinal dilation severity and the amount of ileal length that presented this distended NEC pathology while avoiding potential bias of "grading systems." In NEC pups, the ileum was significantly dilated compared with BF controls (NEC: 1.3 mm, BF: 1.17 mm) (Fig. 3C). hPSC treatment in NEC pups significantly alleviated the ileal distention (NEC-hPSC: 1.21 mm). Additionally, this novel quantification method was used to assess the tissue burden of this pathological dilation (Fig. 3D). Pathological dilation of the ileum was defined as a diameter greater than the BF median diameter plus 2 standard deviations (95% confidence interval). In NEC animals, greater than 25% of the ileum was involved with this gross distention pathology. Upon hPSC treatment, ileal involvement was significantly reduced to less than 10%. Thus, hPSC reduced both the severity of ileal distention and the extent of tissue involvement.

Histological NEC Damage is Ameliorated with hPSC **Administration**

In H&E-stained sections, an average of 2-3 cm of ileum was analyzed for a generalized histopathological scoring of damage on a scale of 0 (normal) to 4 (transmural necrosis) (33). An overall histological score of 2 and above was considered NEC. No morphological changes were observed in BF control pups (NEC Grade: 0) (Fig. 4). In NEC pups, the epithelial layer was disrupted with loss of crypt morphology and varying degrees of cellular and villar sloughing (Fig. 4A). Occasional, localized segments displayed red blood cells within the lumen. After 4 days, 10 of the 11 animals developed NEC for a mean NEC Grade of 2.0 (Fig. 4B). hPSC treatment significantly reduced the NEC-induced damage. Upon hPSC administration, a reemergence of normal crypt/villi morphology and decreased epithelial disruption was observed (Fig. 4A). NEC-hPSC animals had an improved NEC Grade of 1.41 and reduced overall NEC incidence of 9% (Fig. 4B).

In addition to the severity of the NEC Grade, the potential hPSC efficacy in reducing the extent of tissue burden was assessed. In each animal, the percentage of ileal tissue with a Grade of NEC damage (>2) was measured along a total length of 2–3 cm of ileum (% involved = length_{Grade}/total ileal length). On average, \sim 23% of the ileum from each NEC animal had histological damage of NEC Grade ≥2. The NEC damage was predominately Grade 2 (18.2%) with smaller involvement of Grades 3 (4.6%) and 4 (0.1%) (Fig. 4). NEChPSC animals had remarkably reduced ileal involvement with less than 5% of the ileum having histological NEC damage ≥ 2 (Fig. 4). Furthermore, Grade 3 was rarely observed in NEC-hPSC animals with less than 0.5% ileal involvement and no observed Grade 4. These histological findings also correlate with the extent of distention and the "Macroscopic Score" as previously reported (Supplemental Fig. S1) (33). Overall, these analyses show significantly reduced severity in NEC damage and tissue involvement in hPSC-treated NEC animals compared with untreated NEC.

In NEC-hPSC pups, localization of ip-administered hPSC was examined to identify potential modes of action. Utilizing dual-labeled mKATE hPSC in a small cohort of NEC-hPSC pups, IVIS imaging showed bioluminescent signal from labeled hPSC was observed only within the abdomen and not detected

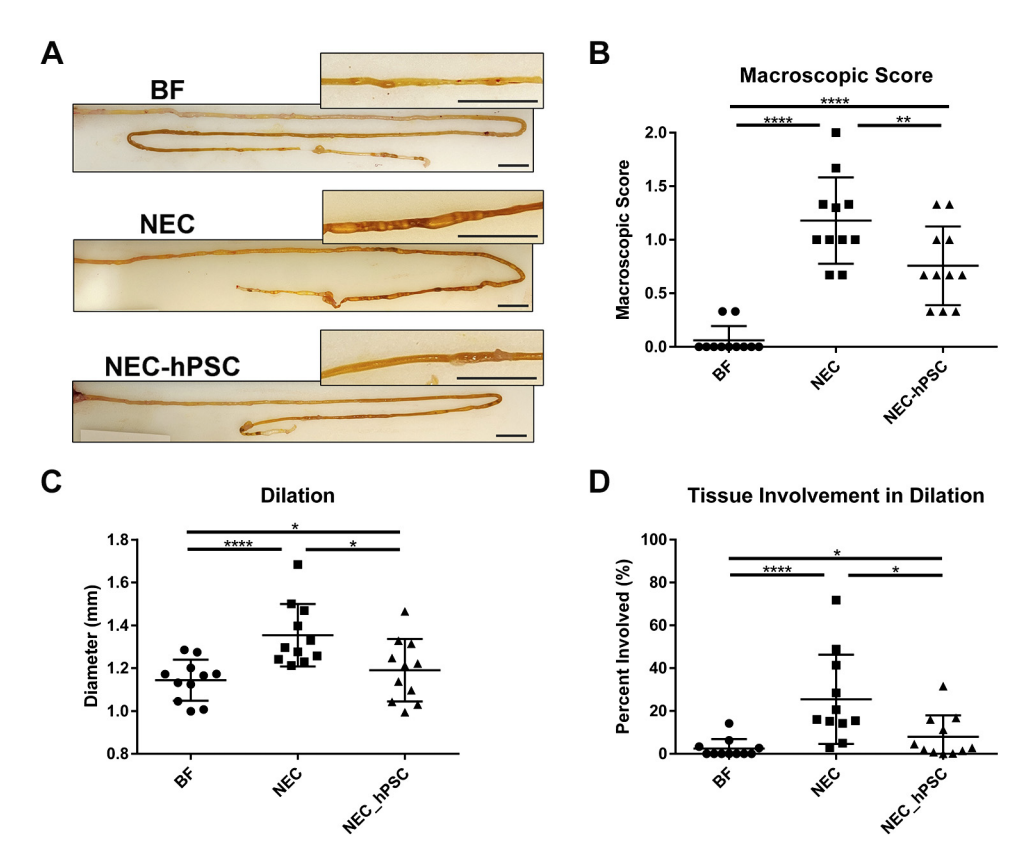


Figure 3. Macroscopic health of ileum. *A*: representative images of the intestine beginning with the duodenum and ending with the colon. Magnified *insets* show the distal ileum of each image. NEC animals have significant ileal distention compared with BF control animals. This distention is reduced in NEC-hPSC animals (each scale bar=1cm). *B*: an established composite macroscopic score that included coloration, consistency, and dilation was used to assess the overall gross pathological health of the ileum (0= healthy, normal). NEC animals have a significantly worse macroscopic score compared with BF controls (NEC=1.18 \pm 0.40; BF=0.06 \pm 0.13, ****P < 0.0001). hPSC treatment reduced the macroscopic pathology of the ileum in NEC-hPSC animals (NEC-hPSC=0.76 \pm 0.37, **P=0.0077). *C*: as the key driving factor of the Macroscopic Score, the severity of ileal dilation was quantified by measuring diameter along the entire length of the ileum. The median of the ileal diameters shows a significant 11% increase (0.13 mm) in NEC animals (NEC=1.30 \pm 0.146 mm; BF=1.17 \pm 0.096 mm, ****P<0.0001). Ileal dilation in NEC-hPSC animals is decreased (NEC-hPSC=1.21 \pm 0.146 mm, *P=0.0348). *D*: to assess the amount of tissue involved, the percent of the ileal length with significant pathological distention was measured. NEC animals had almost a 10.5-fold increase of tissue with pathological distention compared with BF control animals (NEC=25.4% \pm 20.8; BF=2.42% \pm 4.43, ****P<0.0001). hPSC treatment of NEC animals decreased tissue involvement to less than 10% of the ileum (NEC-hPSC=7.95% \pm 10.0; *P=0.0109 vs. NEC and *P=0.0247 vs. BF). Mean values with standard deviation are plotted (n=11 in each group). Statistical comparison by a Kruskal-Wallis analysis followed by post hoc Conover test with Holm family-wise error rate correction for multiple comparisons are available in Supplemental Table S1. BF, breastfed; hPSC, human placental-derived stem cell; NEC, necrotizing enterocolitis.

in the thoracic or head compartments. mKATE hPSC appeared to localize along distinct intestinal outlines in the abdomen at $day\ 4$ (Fig. 5). However, labeled hPSC were not detected in the mucosal layer of the ileum with mKATE immunostaining (data not shown). hPSC engraftment was also not observed in the submucosal and serosal layers. Nonetheless, due to tissue processing procedures that potentially result in some loss of the thin outer layers of the neonatal intestine, very low-frequency engraftment in the outermost serosa or along the intestinal connective tissue could not be completely ruled out. PCR for the human GUS gene was performed to detect the presence of the human-derived hPSC. Human GUS was not detected in NEC-hPSC pups (Fig. 5). These data suggest that hPSC do not engraft in the intestine.

hPSC Treatment Promotes Healing through Attenuation of Epithelial Damage

We sought to investigate the effect of hPSC treatment on inflammation. Previously shown to be associated with NEC,

TNF α , IL-1 β , and NF κ B were selected to investigate the overall inflammatory milieu in the ileum. TNF α expression did not reach statistical significance in the omnibus Kruskal–Wallis test between the three groups. Accordingly, further pairwise comparisons were not conducted for TNF α . However, IL-1 β and NF κ B expression were significantly increased in NEC animals compared with healthy BF controls (Fig. 6A). In NEC-hPSC animals, IL-1 β and NF κ B showed a decreased trend but did not reach statistical significance (Fig. 6A).

We next examined the epithelial damage in NEC by first assessing the crypt/villus architecture in the ileum. The normal villus and crypt structures found in BF ileum were lost in NEC ileum (Figs. 4 and 6*B*). NEC damage caused shortening of villi and shallow crypt invaginations compared with healthy BF ileum (NEC: villus = 91.4 μ m, crypt = 16.8 μ m; BF: villus = 143.8 μ m, crypt = 20.8 μ m) (Fig. 6*B*). hPSC treatment caused significant lengthening of villi (125.7 μ m) (Fig. 6*B*). Moreover, in NEC-hPSC animals, normal crypt depth was increased back to healthy BF control depths (22.1 μ m) (Fig.

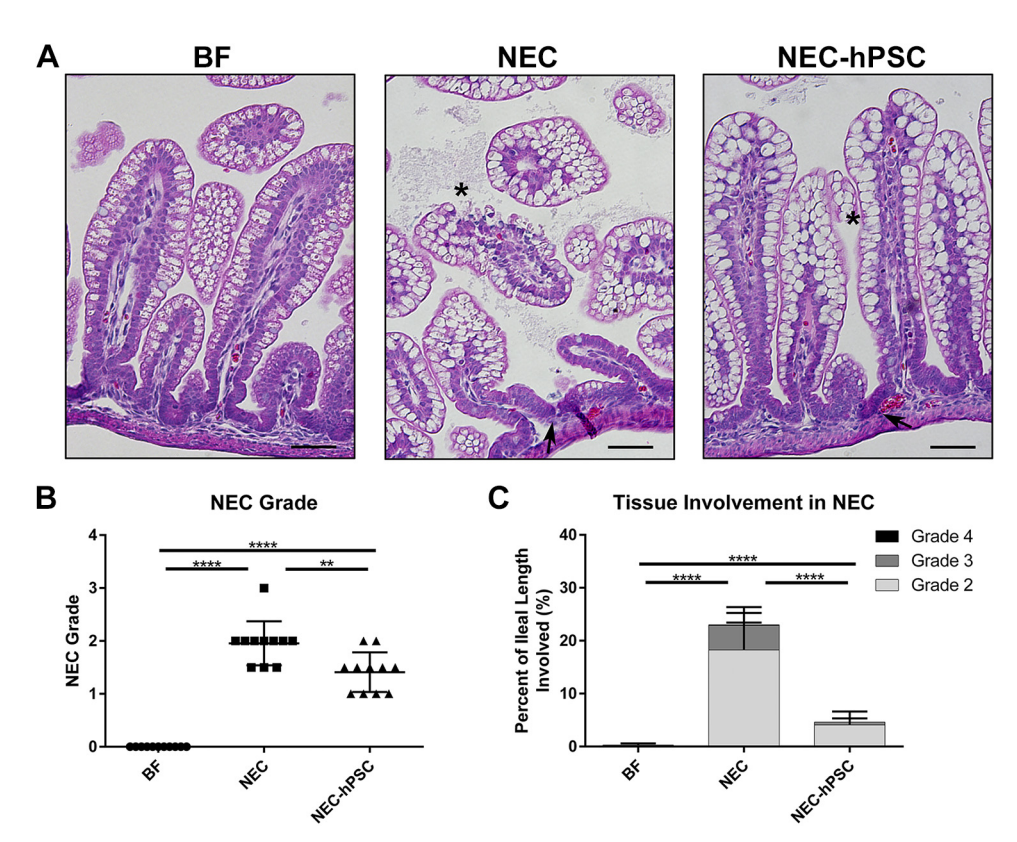


Figure 4. Histological damage in NEC. A: H&E-stained ileal sections show normal histology in BF control animals. NEC animals have loss of normal crypt architecture (arrow), disrupted epithelial cell morphology with cellular sloughing (asterisk), and some villar sloughing. Crypt morphology begins to reemerge in NEC-hPSC animals (arrow). Villi appear more intact with resolving epithelial cell order (asterisk) (scale bar = $50 \,\mu\text{m}$). B: NEC-associated damage in each ileum was assessed using an established histological scoring and given an overall NEC Grade. An NEC Grade ≥ 2 was considered NEC. NEC animals had an increased NEC Grade of 2.0 ± 0.416 compared with BF animals' score of 0.0 ± 0.0 (****P = 0.0001). hPSC treatment of NEC significantly decreased histological NEC damage to 1.41 ± 0.38 (**P = 0.0002 vs. NEC). P = 0.0002 vs. NEC). P = 0.0002 vs. NEC). P = 0.0002 vs. NEC) animals have significantly less tissue with histological damage of NEC Grade P = 0.0002 vs. NEC Grade P =

6*B*). Epithelial turnover was also examined in BF, NEC, and NEC-hPSC ileums. Immunostaining for cleaved caspase 3 showed the low homeostatic apoptosis levels in the epithelium of BF animals (Fig. 6, C and E). The number of apoptotic epithelial cells more than doubled in NEC animals (Fig. 6, C and E). In NEC-hPSC animals, epithelial apoptosis was reduced back to BF amounts (Fig. 6, C and E). To quantify proliferation and cell migration, a subset of animals was ipinjected with EdU 24h before euthanasia at the 96-h end point. Epithelial cell proliferation was decreased in NEC animals (Fig. 6, D and E). Compared with the untreated NEC animals, hPSC-treated NEC animals had a significant increase in epithelial proliferation (Fig. 6, D and E).

hPSC Treatment Supports Enterocytes and The Intestinal Stem Cell Niche in NEC Repair

Loss of critical epithelial cell lineages was assessed using immunostaining with lineage-specific antibodies [Ezrin, Lysozyme, SOX9, and OLFM4 (42)]. Ezrin immunoreactivity was used to quantify enterocytes in the ileum normalized by the linear intestinal length measured (Fig. 7, *A* and *C*). BF controls had normal, ordered enterocytes lining villi with

 \sim 1,013 enterocytes/mm. In NEC, a decrease of Ezrin $^+$ enterocytes was observed (701 enterocytes/mm). As suggested by improved villar height, hPSC therapy significantly increased enterocyte numbers (882 enterocytes/mm); however, it did not completely replenish cell numbers back to BF levels.

To next assess the intestinal stem cell niche within the crypt, LGR5⁺ intestinal stem cells and Paneth cells were quantified with immunostaining for OLFM4 [a marker of LGR5⁺ stem cells (42)] and Lysozyme (mature Paneth cells) (Fig. 7, A, B, D, and E). Compared with BF controls, NEC animals had a significant loss of LGR5⁺ stem cells (BF: 61.7 cells/ mm: NEC: 19.3 cells/mm) (Fig. 7D). Upon hPSC treatment. LGR5⁺ stem cells were significantly increased compared with untreated NEC animals (40.6 cells/mm) (Fig. 7D). Loss of Paneth cells have been reported to lead to NEC onset (14). In our NEC rat model, Paneth cells are still undergoing expansion and are not observed within each crypt of BF control ileum. Therefore, we quantified Lyz immunostaining in larger length of ileum (4-8 mm) than used for the previous quantifications (1-1.5 mm). Paneth cells were observed at a rate of 14.5 cells/mm in healthy BF animals (Fig. 7E). In NEC animals, Paneth cells are significantly lost with only 8.0 cells/mm (Fig.

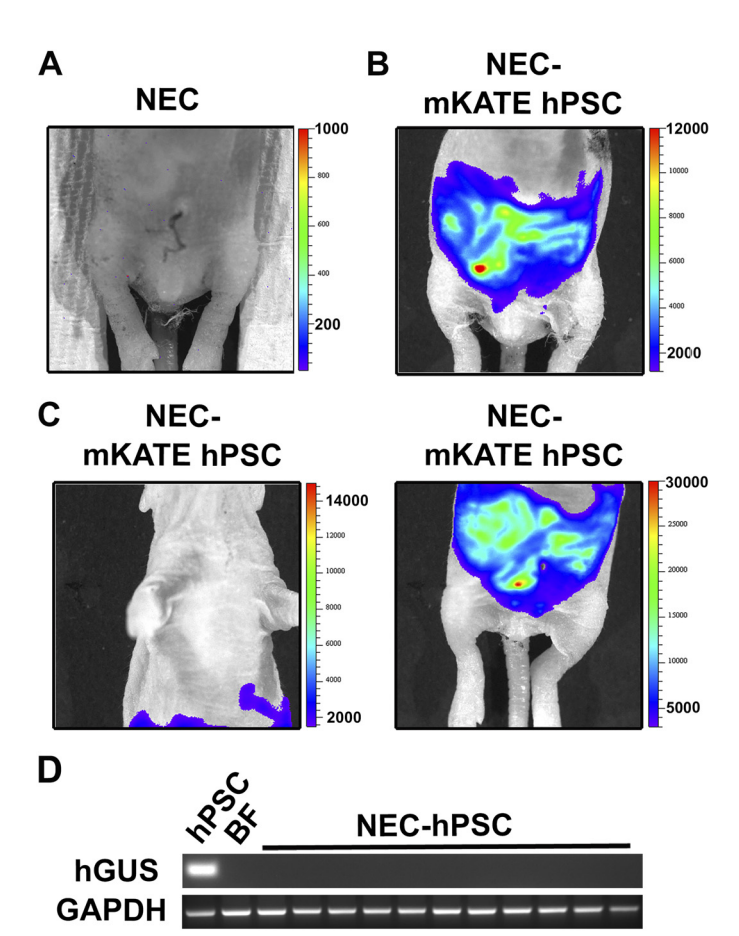


Figure 5. Localization of intraperitoneally administered hPSC. In A, B, and C, IVIS imaging was for live cell tracking of dual-labeled hPSC. A: an untreated NEC pup was used as a negative control and shows no bioluminescent signal during IVIS imaging. B: a NEC pup received dual-labeled mKATE hPSC at the first cell injection. IVIS imaging before euthanasia on day 4 shows the bioluminescent signal from mKATE hPSC is located along distinct intestinal outlines in the abdomen. Intense red spot is the site of injection. C: in a second mKATE hPSC-treated pup, no signal was detected in the thoracic compartment. However, mKATE hPSC were observed within the abdomen and appeared to outline sections of the intestine. D: PCR of human GUS was used to detect the presence of human cells within the rat tissue of NEC-hPSC pups that received unlabeled hPSC. hPSC were used as a positive control, whereas BF pups that received only saline injections served as a negative control. None of the 11 NEC-hPSC pups had detectable amounts of human GUS. This suggests hPSC did not fully engraft into the ileum. GAPDH that detects both the human and rat gene served as a positive sample control. BF, breastfed; hPSC, human placental-derived stem cell; NEC, necrotizing enterocolitis.

7*E*). Similar to LGR5 $^+$ stem cells, the Paneth cell population was significantly increased (19.1 cells/mm) with hPSC treatment (Fig. 7*E*).

SOX9 and β -catenin immunostaining were then performed to further examine the intestinal stem cell niche and a potential role of WNT signaling. As a broadly expressed marker of intestinal stem and progenitor cells and of a subset of Paneth cells (43, 44), SOX9 $^+$ cells were abundantly observed in BF pups (266 cells/mm) (Fig. 8). SOX9 $^+$ cells were significantly reduced by almost half in NEC damage. However, this cell population was restored to normal levels with hPSC therapy (260 cells/mm) (Fig. 8). Previous studies have shown the essential role of WNT signaling in SOX9

expression and crypt cell dynamics (45, 46). Thus, we examined the presence of nuclear localization of β -catenin (a marker of activated WNT) within crypt cells. We quantified nuclear β -catenin⁺ cells and total crypt cells in well-oriented crypts and accordingly normalized quantifications per crypt. In BF pups, nuclear β -catenin was observed in eight cells per crypt, which equated to 64% of the crypt cells (percentage represents ratio of nuclear β -catenin⁺ cells per total crypt nuclei) (Supplemental Fig. S2). The total number of nuclear β -catenin⁺ crypt cells was reduced in NEC pups (4.9 cells/crypt). Further, these positive cells represented only 38% of the crypt cells. Upon hPSC therapy, nuclear β -catenin⁺ cells were present in similar levels to BF controls (7.2 cells/crypt, 70.3%) (Supplemental Fig. S2).

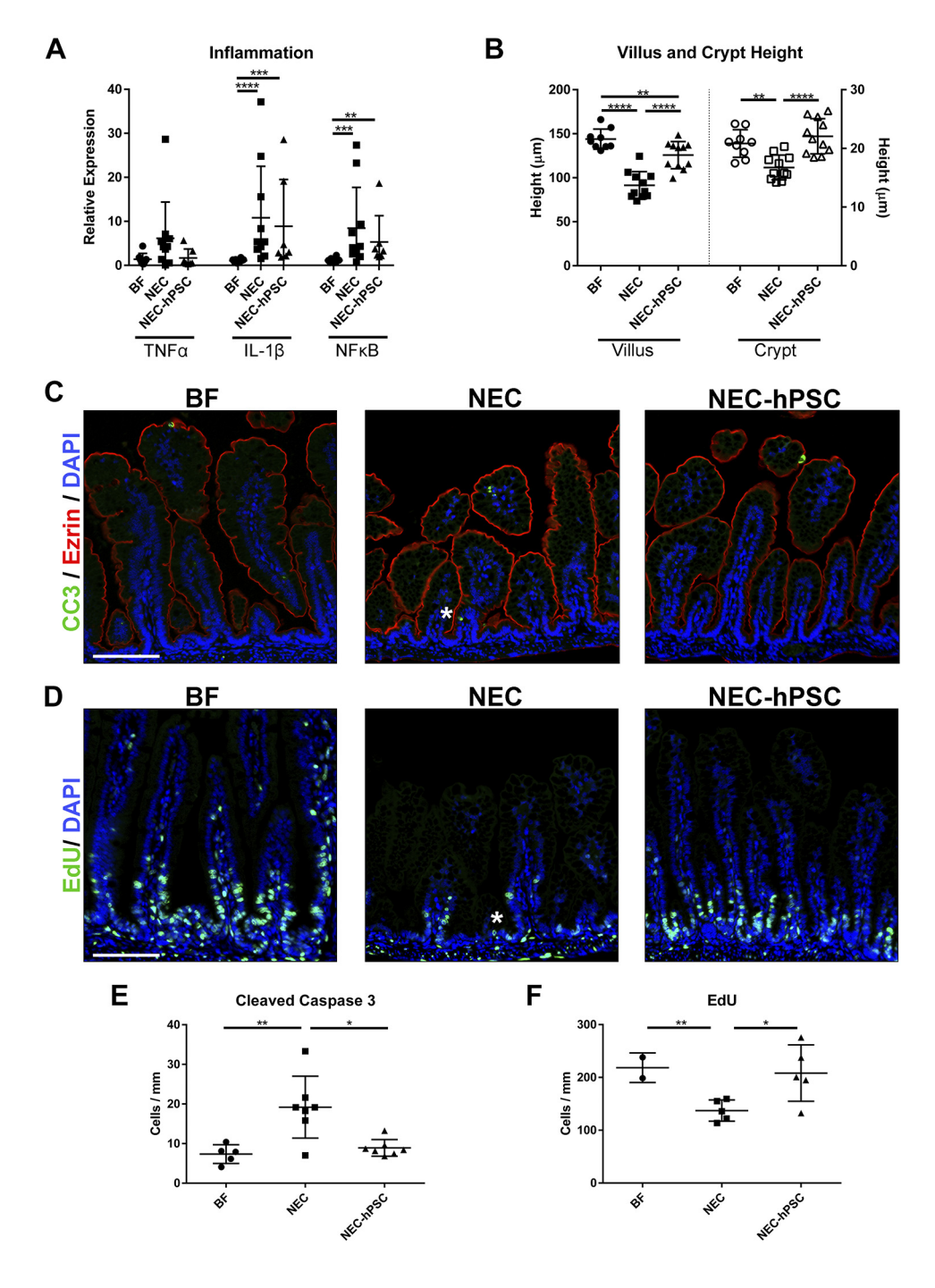
While LGR5⁺ stem cells and Paneth cells always reside within the crypts, the distribution of other cellular features may lend insight into the epithelial dynamics in NEC-hPSC animals. Therefore, we examined the cellular distribution of Ezrin⁺ enterocytes, EdU⁺, and cleaved caspase 3⁺ cells along the crypt-villus axis (Supplemental Fig. S3). Localization of LGR5⁺ stem cells was used as a localization control as their cellular position remains mostly unchanged within the crypt. First, localization of EdU+ epithelial cells was assessed to examine potential cellular migration of the recently proliferating cells. Histograms of EdU⁺ cell distribution show proliferating cells in BF animals migrate out of the crypts toward the villus tip with occasional EdU⁺ cells found further up the villi (Supplemental Fig. S3). In NEC animals, EdU⁺ cells appear to have reduced migration from the crypts. While the number of EdU⁺ cells increases with hPSC therapy, most of these cells are localized near the crypts with relatively none observed up the villi as observed in BF animals (Supplemental Fig. S3). In contrast, apoptotic epithelial cells were more widely dispersed along the crypt-villus axis (Supplemental Fig. S3). One increased region of apoptotic cells within the villi was noted in NEC animals. When comparing enterocyte distributions between NEC and NEC-hPSC animals, NEC animals displayed a decrease in enterocytes in the same general villar localization as the aberrant apoptosis. This may suggest that increased apoptosis within this villar region corresponds with the decrease in enterocytes and resultant shortened villar height. As EdU⁺ cells do not rapidly migrate up the villi in NEC-hPSC animals, the increase in enterocytes beginning at this same localization may be the result of the observed resolution of this aberrant apoptosis rather than simple replenishment via newly divided cells. As expected, LGR5⁺ stem cells, SOX9⁺ cells, and Paneth cells (not shown) showed increased numbers of cells but no changes in distribution between animal groups with localization consistently within the crypts. Together, this in-depth distribution analysis yields insight into the complex interplay of cellular changes that occur in enterocytes along the villi in addition to the intestinal stem cell niche depletion and expansion. Further, this method provides an additional tool for future analysis of the complex cellular dynamics involved in cessation and repair of NEC damage.

DISCUSSION

In the past decade, researchers have made significant advances in identifying important prophylactic strategies for

reducing the risk of NEC onset (17, 47). Unfortunately, few approaches have demonstrated the therapeutic ability to ameliorate established NEC damage. To address this gap, we focused our present study on the potential of hPSC for NEC treatment. In the neonatal rat model of NEC, intestinal damage is induced within 24–36 h from the start of the NEC stressors (31–33) and confirmed through observations of clinical symptoms onset shown in Fig. 2. Because of increasing mortality rates, this model is limited to a 96-h end point. Based on these timings, our present study time line included hPSC injection following the conclusion of LPS administration. While this resulted in a shortened treatment timetable, it did

enable investigation of therapeutic benefits as NEC intestinal damage is known to be induced before the treatment timing. An additional challenge for NEC therapeutic studies is clinical application, specifically pertaining to the staging of the disease, timing of intervention, and the route of administration. In this study, we sought to examine the potential for intervention in earlier stages of NEC that would reflect the Modified Bell's Stages I and II in human NEC. We postulated that earlier intervention may be better tolerated in the infant and, further, may decrease NEC progression to advanced stages that require surgery. Therefore, we focused our animal model to reproducibly develop NEC Grade 2



damage to specifically investigate early clinical NEC intervention in this study. While this earlier stage of NEC damage in our study may mask the full therapeutic capacity of hPSC, this focus on early NEC Stages yields more insight into potential early clinical application for medically managed NEC. Therapeutic options for advanced NEC Stages remain a significant need and future studies can now directly focus on the hPSC therapeutic capacity for severe NEC damage. The route of administration is another important challenge in the clinical application of therapeutics, especially in premature infants. Intravenous administration of cell therapies is associated with cell entrapment and embolism risks in the lungs (48, 49). Therefore, we sought an alternative administration route to avoid these potential risk factors in premature infants already predisposed to lung impairment. Previous studies have supported the safety and efficacy of intraperitoneal (ip) injection for cell therapy including preclinical NEC investigations (50-52). Considering these clinical translation factors, the ip route of administration was chosen to balance the potential risks and benefits in this unique patient population.

In this study, we examined the therapeutic effects across the multiple scales ranging from whole animal clinical symptoms to histological cellular damage using comprehensive quantitative analyses at each length scale. At the cellular level, the villi/crypt morphologies and essential epithelial cell populations were reestablished in hPSC-treated NEC pups. As assessed by the "NEC Grade," the overall severity of histological damage across the ileum was significantly decreased. This cellular-level amelioration extended to observe improvement at the macroscopic level. Upon gross examination, the "Macroscopic Score" that included fragility and distention was decreased in hPSC-NEC ileum. The extent of ileal tissue involved in both the histological damage and the pathological dilation were also significantly reduced. However, these tissue-level recoveries did not correlate to full resolution of whole animal clinical symptoms. Although trending toward improvement, body weight and Clinical Sickness Score did not reach statistical significance by the 96-h end point. A previous study using amniotic fluid stem cells for NEC treatment has shown whole animal improvements with cells administered at 24 h (25, 53). Our current study was designed with an 8-h increase in NEC initiation and established (31-33) before our treatment time point. The resultant shortened treatment window and our focus on earlier NEC stages could be contributing reasons for the lack of statistically significant clinical resolution at the study end point. We also specifically utilized human-derived PSC to maintain clinical relevance; however, potential decreased efficacy due to the species mismatch should also be considered. Furthermore, as the hPSC therapeutic effect occurred without cell engraftment, a concentrated hPSC secretome administration may also increase therapeutic effects, in addition to allowing for other safe possibly more direct routes of administration. Additionally, other nonintestinal organs have been shown to contribute to advancing NEC pathogenesis and long-term adversities (54–56). Future studies of "extraintestinal" effects of hPSC therapy may lend insight into potential therapeutic benefits for nonintestinal damage in addition to addressing the gap between observed tissue-level improvement and lack of whole animal clinical symptom resolution.

NEC is characteristically a multifocal disease in the premature ileum. With current medical management during early-stage NEC, over 30% of patients progress to advanced disease requiring surgical intervention to remove necrotic segments (57). This unpredictable progression correlates with drastically increased mortality rates (up to 50%) (58, 59). For survivors, surgical management is also compounded by long-term complications associated with the amount of remaining healthy bowel remaining (60-63). Therefore, both the severity and tissue burden of NEC are important factors in assessing potential therapies. hPSC therapy decreased the amount of tissue involved in pathogenic NEC damage to less than 5%. Moreover, an NEC Grade of 3 or above was rarely observed. If translated into a clinical setting, this could result in a smaller portion of bowel removed or possible avoidance of surgery for some patients. The reduction of surgical interventions alone could significantly impact outcomes for patients with NEC. In humans, impaired motility, dysbiosis, and malabsorption are associated with NEC pathogenesis and significant ileal distention (64–66). In animal studies, this ileal distention can also

Figure 6. Assessment of inflammation and epithelial barrier. A: quantitative PCR for three prominent inflammatory signaling biomarkers (TNF α , IL-1 β , and NFκB) was performed to examine global inflammatory status. IL-1β and NFκB were significantly increased in NEC animals compared with BF control animals (NEC: IL-1 β = 10.18 ±11.71, ****P < 0.0001; NFκB = 8.44 ± 9.27, ***P = 0.0004). Neither of these two inflammatory biomarkers were significantly reduced with hPSC treatment and remained elevated compared with BF animals (NEC-hPSC: IL-1 β = 8.89 ± 10.61, ***P = 0.0002; NFxB = 5.31 ± 5.98, **P = 0.0032). TNFα did not reach statistical significance in the omnibus Kruskal–Wallis test and thus could not be used for pairwise comparisons. B: villus and crypt heights were measured to assess overall epithelial status. In NEC, villi and crypts were significant shorter compared with BF controls (NEC: villus = $91.4 \pm 15.5 \,\mu\text{m}$, crypt = $16.8 \pm 2.1 \,\mu\text{m}$; BF: villus = $143.8 \pm 11.5 \,\mu\text{m}$, crypt = $20.8 \pm 2.3 \,\mu\text{m}$; *****P < 0.0001, **P = 0.0012, respectively). While NEC-hPSC villar height was not completely restored to BF levels by day 4 (**P = 0.0057), it was significantly increased compared with NEC animals (125.7±15.4 µm, ****P < 0.0001). The crypt height in NEC-hPSC was also increased (22.1±3.0 µm ****P < 0.0001 vs. NEC). Notably, NEC-hPSC height was restored back to BF levels. C: immunostaining for cleaved caspase 3 (green) showed increased apoptosis in NEC animals (asterisk). This aberrant cell death was not observed in NEC-hPSC animals (Ezrin = Red, DAPI = blue, scale bar = 100 μm). D: EdU (green) was used to identify proliferation in a subset of animals. NEC animals had marked decrease in proliferating cells emerging from the crypts (asterisk). In NEC-hPSC, normal proliferation and migration began to reemerge (arrow) (scale bar = 100 μm). E: quantification of epithelial cells positive for nuclear cleaved caspase 3 shows a significant increase in epithelial cell apoptosis in NEC (19.2 ± 7.8 cells/mm, **P = 0.0073 vs. BF). Aberrant apoptosis is decreased in NEC-hPSC (8.9 ± 2.1 cells/mm, *P = 0.0306 vs. NEC) and reduced to normal BF levels (7.3±2.4 cells/mm). F: proliferation denoted by EdU incorporation was quantified in epithelial cells. Proliferation is reduced in NEC (137.2 \pm 20 cells/mm, **P = 0.0075 vs. BF). Upon hPSC treatment of NEC, epithelial proliferation is significantly increased compared with untreated NEC animals (NEC-hPSC: 208.2 ± 53.44 cells/mm, *P = 0.0372 vs. NEC). Mean values with standard deviation are plotted (n for each analysis is denoted in dot scatter plots). Statistical comparison by a Kruskal-Wallis analysis followed by post hoc Conover test with Holm family-wise error rate correction for multiple comparisons are available in Supplemental Table S1. BF, breastfed; DAPI, 4',6-diamidino-2-phenylindole; hPSC, human placentalderived stem cell; NEC, necrotizing enterocolitis.

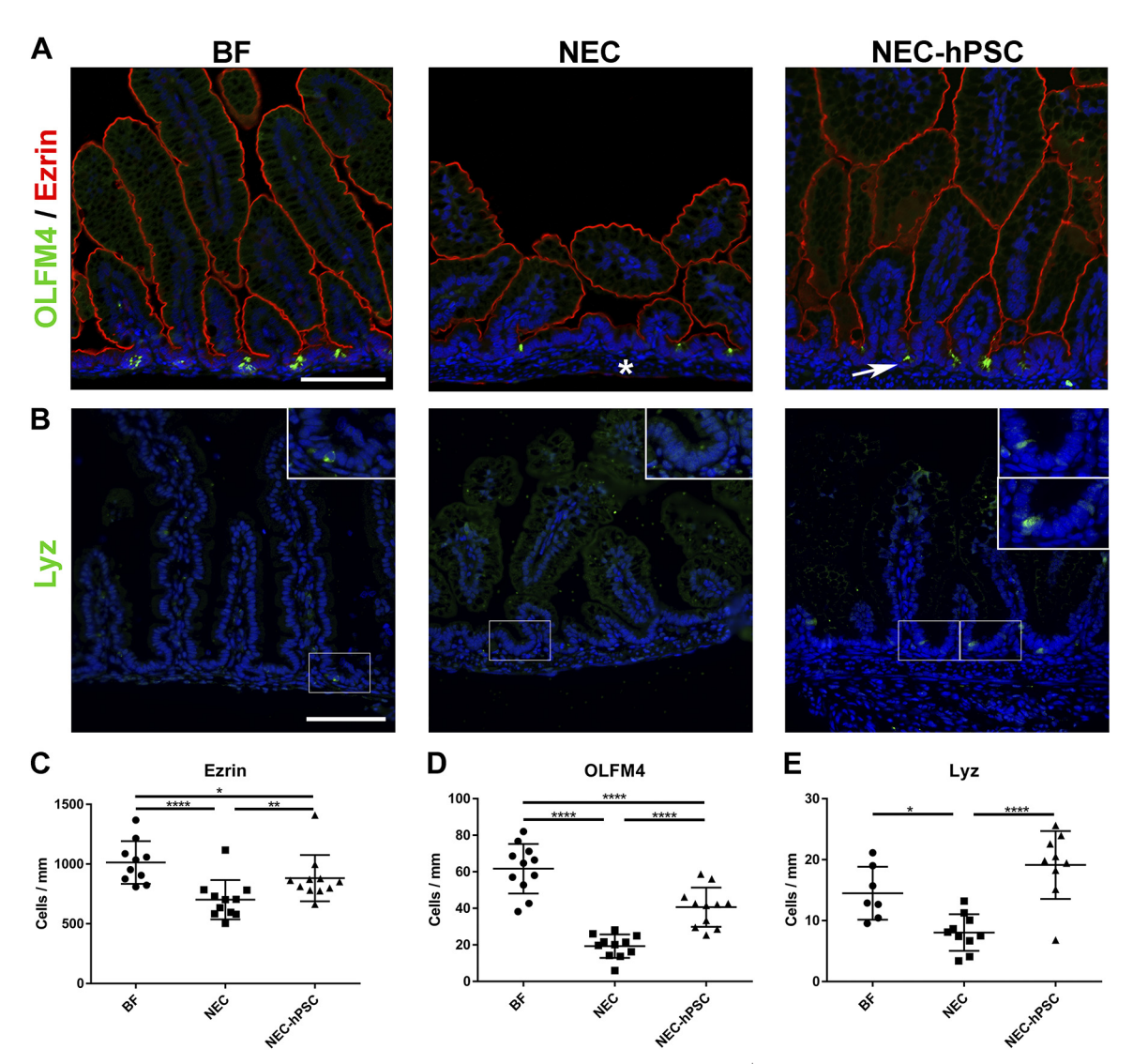


Figure 7. Assessment of epithelial cell lineages. A: immunostaining for Ezrin (red) and the LGR5 $^+$ intestinal stem cell (ISC) marker OLFM4 (green) illustrated the shortened villi and crypt heights in NEC. Further, it showed a loss of both enterocytes and LGR5 $^+$ stem cells (asterisk) in NEC that was partly ameliorated with hPSC treatment (arrow) (DAPI = blue, scale bar = 100 μ m). B: immunostaining for Lyz (green) demonstrated the few Paneth cells in the developing intestine in BF pups that are further reduced in NEC. However, hPSC therapy increased the number of Paneth cells (DAPI = blue, scale bar = 100 μ m). C: quantification of Ezrin $^+$ enterocytes showed significant loss in NEC (701.6 \pm 164.3 cells/mm) compared with BF controls (1,013 \pm 178.6 cells/mm, ****P < 0.0001 vs. NEC). In NEC-hPSC animals, enterocytes are increased (882 \pm 193.5 cells/mm, ***P = 0.0095) but do not reach full normal BF levels by day 4 (*P = 0.0372). D: OLFM4 $^+$ cells were quantified to assess the presence of LGR5 $^+$ ISC within the crypts. As reflected in the reduce crypt height, LGR5 $^+$ ISC are significant lost in NEC (19.3 \pm 6.4 cells/mm vs. BF = 61.7 \pm 13.5 cells/mm, ****P < 0.0001). With hPSC treatment, LGR5 $^+$ ISC reemerge with a significantly increased population (40.6 \pm 10.8 cells/mm, ****P = 0.0001) compared with NEC animals. However, they are not completely restored to BF amounts (****P < 0.0001). E: while the Paneth cell population is not fully developed in neonates, previous studies have shown their importance in sustaining the ISC niche and in NEC. Larger sections of lysosyme-immunostained ileum were scanned to more accurately quantify the sparse, developing Paneth cell population. NEC animals had a significant decrease in Paneth cells (8.0 \pm 3.0 cells/mm vs. BF = 14.5 \pm 4.3 cells/mm, *P = 0.0106). Paneth cells were significantly increased to slightly above BF levels in NEC animals treated with hPSC (19.1 \pm 5.6 cells/mm, ****P = 0.0001 vs. NEC). Mean values with standard deviation are

be used as a biological readout of intestinal health and thus we sought to further investigate its severity and extent. As the NEC distention was observed in a multifocal pattern along the length of the ileum, a custom software was developed to automate the quantification of both the severity of distention and the percent of ileal tissue involved in this "patchy" pathology. A comparison of this gross pathology to the histological damage analysis

also revealed a similar percentage of tissue involved in each. This finding supports a previously reported correlation between the severities of the "Macroscopic Score" as an indicator of the "NEC Grade" (33). While previously used composite scores can give an overall assessment of the tissue, more in-depth quantitative analysis of tissue involvement can be beneficial when investigating a multifocal disease such as NEC. This newly developed

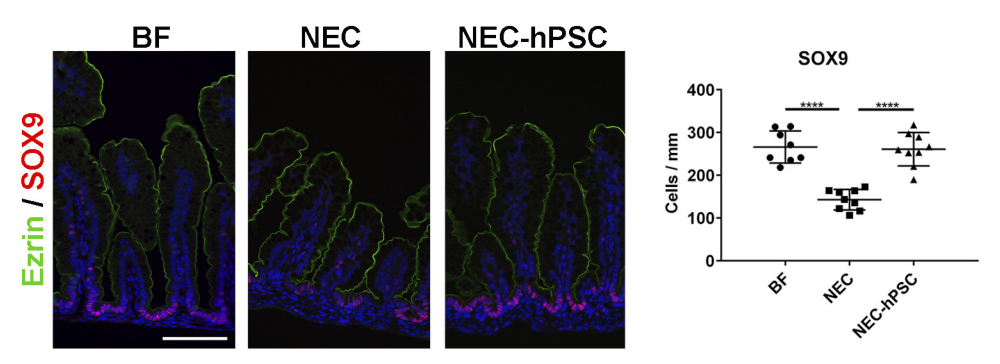


Figure 8. Assessment of the intestinal stem cell niche and signaling. Immunostaining of SOX9 (red) and Ezrin (green) shows abundant SOX9⁺ cells in BF pups (266± cells/mm). SOX9 + cells were significantly reduced in NEC (142.8± cells/mm, ****P < 0.0001). Upon hPSC treatment, these cells were restored back to normal levels (260.8 \pm cells/mm, ****P < 0.0001 vs. NEC) (DAPI = blue, scale bar = 100 μ m). Mean values with standard deviation are plotted (n for each analysis is denoted in dot scatter plots). Statistical comparison by a Kruskal-Wallis analysis followed by post hoc Conover test with Holm family-wise error rate correction for multiple comparisons are available in Supplemental Table S1. BF, breastfed; DAPI, 4',6-diamidino-2-phenylindole; hPSC, human placental-derived stem cell; NEC, necrotizing enterocolitis.

software for automated pathological distention measurements now provides a novel research analysis tool that reduces bias, increases throughput, and allows for more complete multilevel comparisons of NEC damage in future studies.

As NEC is a multifactorial disease involving several instigating factors, multiple potential therapeutic targets have been posited. Of these, reduction of the overreactive immune response is a common focus of therapeutic strategies, as it plays a significant role in not only intestinal NEC damage but also systemic sepsis. However, clinical application is a challenge for NEC therapeutics that target narrow suppression of the pathogenic inflammation. For example, inhibitors that suppress TNF α have shown the apeutic ability in preclinical NEC models (67) but also pose an uncertain risk of systemic side effects (i.e., further infections) in an already vulnerable patient population (68). Perinatal stem cells present a unique approach known for immune modulation rather than specific inflammatory cytokine suppression (69, 70). hPSC also uniquely secrete a multitude of factors that can target other components of NEC pathogenesis via potent paracrine signaling (29, 71, 72). Therefore, we hypothesized that hPSC therapy was a novel multifaceted paracrine approach that could improve epithelial damage and reduce global pathogenic inflammation in NEC disease. As discussed above, hPSC therapy improved NEC damage as the result of potentially two synergistic sources: prevention of disease progression and promotion of epithelial recovery. To examine changes in the pathogenic inflammation, we used a panel of the three prominent inflammatory biomarkers associated with NEC pathogenesis: TNF α , IL-1 β , and NF κ B (7, 32, 73–75). In the ileum, increased IL-1β and NFκB levels in NEC animals did not reach statistical significance in their decreasing expression trend upon hPSC treatment. Additionally, TNFα did not yield any significant differences in our studies. While we expected broad reduction in these overarching inflammatory biomarkers, the mild declining trends suggest that hPSC therapy does not reduce the overall pathogenic inflammatory milieu at this stage of NEC disease. Thus, hPSC do not induce NEC healing through potent reduction of all pathogenic inflammation. Conversely, recent studies have shown an increase in

specific reparative immune pathways during NEC recovery in patients (7, 76) that is not always accompanied by a significant loss of the pathogenic inflammatory components. Our focus on broad inflammatory cytokines may not detect more targeted immune modulatory effects of hPSC. Therefore, future studies should investigate the specific reparative immune pathways not examined in the present study. While NEC is traditionally thought of as a heavily immune-driven disease, these current data in pathogenic inflammation suggest that support of epithelial repair can also be an effective target in NEC treatment approaches.

One of the most prominent findings in our present study is the significant improvement of the intestinal stem cell and crypt niche, specifically the SOX9⁺ stem/progenitor cell, LGR5⁺ stem cell, and Paneth cell populations. Recent studies have begun to highlight the importance of these epithelial cell lineages in NEC. In in vitro studies with NEC enteroids, stimulation of LGR5+ stem cells with exogenous Wnt3a was shown to promote epithelial survival and growth (77, 78). Without exogenous Wnt3a administration, fewer NEC enteroids survived in culture. Paneth cells are endogenous sources of Wnt signaling that supports LGR5+ stem cells in healthy crypts. Loss of Paneth cells coupled with bacterial colonization in neonate mice lead to the onset of characteristic NEC disease (14). Furthermore, SOX9 is a target of Wnt signaling and plays an important role in Paneth cell differentiation and maintenance of the intestinal stem cell niche (44, 45). These investigations have begun to reveal the importance of Paneth cells, LGR5⁺ stem cells, and SOX9⁺ stem/progenitor cells in prevention and recovery of NEC damage. In our NEC animal model, the observed loss of Paneth cells, LGR5⁺ stem cells, and SOX9+ stem/proge-nitor cells in NEC was ameliorated upon hPSC treatment. Similarly, hPSC restored the total number and percentage of nuclear β-catenin⁺ crypt cells. Previous studies have shown a connected cascade of Wnt signaling via β -catenin that can lead to an increase in intestinal stem cell proliferation in addition to a targeted increase in SOX9 expression that promotes Paneth cell differentiation (43, 45, 79). As our data show the central factors in this signaling cascade are increased with hPSC treatment, further investigations into this β-catenin/Wnt activated signaling as a

potential mechanism of hPSC treatment of NEC damage are warranted. Overall, our current findings coupled with the observed lack of potent reduction in pathogenic inflammation suggest the stem cell and Paneth cell niche support is a key mechanism of action utilized by hPSC therapy.

In intestinal injuries associated with stem cell niche loss, several signaling pathways in addition to Wnt have been identified to support the subsequent repair of the niche. In wound healing of ulcerated lesions, localization of Cox2expressing cells abutting the crypt is essential for epithelial repair and replenishment (80). A role for crypt-adjacent stromal Cox2⁺ cells has also been suggested in amniotic fluid stem cell treatment of experimental NEC (25). Thus, a similar pathway may also be utilized by hPSC therapy to repair the intestinal stem cell niche with NEC damage. In addition, hPSC have been recently shown to uniquely express EGF receptor (EGFR) and NRG1, members of the EGFR/ErbB signaling pathways (29). Activation of EGFR via breast milk exposure is a prominent protective pathway in the neonatal intestinal epithelium. Notably, exogenous dosing of EGFR activating ligands can protect against NEC onset but fail to repair established experimental NEC damage (21, 52). The therapeutic insufficiency of exogenous ligand dosing may be due to the significant reduction of EGFR expression that occurs in NEC pathogenesis (18). However, previous studies have demonstrated the ability of secreted EGFR-containing exosomes to increase EGFR expression and possibly amplify downstream signaling in recipient cells (81, 82). Further studies are needed to investigate whether this can occur with hPSC-secreted EGFR into NEC damaged tissue, specifically LGR5⁺ stem cells. In a similar signaling pathway, hPSC also express NRG1 (29), a ligand for the Erb4 receptor in the EGFR/Erb receptor kinase family. In cultured mouse ileal enteroids, Erb4 loss via genetic deletion reduces the Paneth cell population. Further activation of Erb4 in an experimental NEC model protected the Paneth cell lineage. As we observed significant expansion of Paneth cells, hPSC may also signal through the EGFR/ErbB family to protect or increase Paneth cell lineage in addition to the potential pathway of SOX9-supported Paneth cell differentiation. In addition to these more well-known pathways in NEC, several other factors have been found in the hPSC secretome such as Lactoferrin, ICAM-1, EpCam, and Integrin β1 that can target intestinal stem cells in homeostasis and other intestinal diseases (23, 29). Altogether, hPSC possess a plethora of potential signaling pathways including both direct to epithelium signaling and indirect cellular interactions. These hypothesized pathways along with the β-catenin/Wnt signaling pathway suggested by the current data represent potential mechanisms of action that individually or synergistically can support the observed stem cell niche restoration. Additionally, our data suggest hPSC can ameliorate intestinal repair via distant paracrine signaling, further supporting the hPSC secretome as a mode of action for NEC repair. While future studies can further elucidate the pivotal hPSC signaling pathways, the findings here establish that the paracrine support of the intestinal stem cell niche is one mode of action of hPSC treatment for NEC disease.

In conclusion, hPSC therapy can ameliorate established NEC damage at the cellular and tissue level in the NEC animal model. While broad reduction in pathogenic inflammatory cytokines was not observed, significant epithelial and stem cell niche amelioration corresponding to improved macroscopic health was induced with hPSC treatment. As perinatal stem cell therapies have shown low long-term engraftment rates into the intestine (25) and we saw no hPSC engraftment in the intestine, it is reasonable to conclude that hPSC therapy functions via potent paracrine signaling similar to that observed in previous studies (25, 29). In phase I clinical trials, perinatal stem cells appear to have an acceptable safety profile for use in premature infants (83-85). Therefore, these findings demonstrate hPSC are a unique approach that should be further investigated for clinical translation as an NEC therapeutic strategy. Future studies of hPSC-based therapy will include in-depth investigations into potential reparative immunomodulation, hPSC secretome administration (i.e., conditioned media, exosomes) to safety and potency, and treatment of advanced NEC Stages. Additionally, hPSC provide a critical research tool that can be utilized to elucidate the necessary mechanisms in the prevention of progression and repair to expand our overall understanding of neonatal repair pathophysiology.

ACKNOWLEDGMENTS

The Ezrin antibody developed by Clinical Proteomics Technologies for Cancer was obtained from the Developmental Studies Hybridoma Bank, created by the National Institute of Child Health and Human Development of the National Institutes of Health and maintained at The University of Iowa, Department of Biology, Iowa City, IA. We thank Dr. Frank Marini and Kristina Stumpf for assistance with the Nuance system for immunofluorescent imaging. We also thank the Regenerative Medicine Clinical Center at Wake Forest Institute for Regenerative Medicine for providing the human placental-derived stem cells.

GRANTS

These studies were supported by the state of North Carolina (to A. Atala), Lisa Dean-Moseley Foundation (to M. Z. Schwartz and V. G. Weis), and NIH-NCI K25CA204599 (to J. A. Weis).

DISCLOSURES

No conflicts of interest, financial or otherwise, are declared by the authors.

AUTHOR CONTRIBUTIONS

V.G.W., M.Z.S., C.C., and A.A. conceived and designed research; V.G.W., A.C.D., G.M., C.C., M.G., E.W., and J.A.W. performed experiments; V.G.W., A.C.D., C.B.P., and J.A.W. analyzed data; V.G.W., M.Z.S., and A.A. interpreted results of experiments; V.G.W. prepared figures; V.G.W. drafted manuscript; V.G.W., M.Z.S., and A.A. edited and revised manuscript; V.G.W., A.C.D., G.M., C.C., M.G., E.W., C.B.P., J.A.W., M.Z.S., and A.A. approved final version of manuscript.

REFERENCES

Fanaroff AA, Stoll BJ, Wright LL, Carlo WA, Ehrenkranz RA, Stark AR, Bauer CR, Donovan EF, Korones SB, Laptook AR, Lemons JA, Oh W, Papile L-A, Shankaran S, Stevenson DK, Tyson JE, Poole WK; NICHD Neonatal Research Network. Trends in neonatal morbidity and mortality for very low birthweight infants. Am J Obstet Gynecol 196: e141-e148, 2007. doi:10.1016/j.ajog.2006.09.014.

- Horbar JD, Carpenter JH, Badger GJ, Kenny MJ, Soll RF, Morrow KA, Buzas JS. Mortality and neonatal morbidity among infants 501 to 1500 grams from 2000 to 2009. *Pediatrics* 129: 1019–1026, 2012.
- MohanKumar K, Namachivayam K, Chapalamadugu KC, Garzon SA, Premkumar MH, Tipparaju SM, Maheshwari A. Smad7 interrupts TGF-β signaling in intestinal macrophages and promotes inflammatory activation of these cells during necrotizing enterocolitis. *Pediatr Res* 79: 951–961, 2016. doi:10.1038/pr.2016.18.

doi:10.1542/peds.2011-3028.

- Egan CE, Sodhi CP, Good M, Lin J, Jia H, Yamaguchi Y, Lu P, Ma C, Branca MF, Weyandt S, Fulton WB, Nino DF, Prindle T Jr, Ozolek JA, Hackam DJ. Toll-like receptor 4-mediated lymphocyte influx induces neonatal necrotizing enterocolitis. J Clin Invest 126: 495– 508, 2016. doi:10.1172/JCl83356.
- Maheshwari A, Kelly DR, Nicola T, Ambalavanan N, Jain SK, Murphy-Ullrich J, Athar M, Shimamura M, Bhandari V, Aprahamian C, Dimmitt RA, Serra R, Ohls RK. TGF-β2 suppresses macrophage cytokine production and mucosal inflammatory responses in the developing intestine. *Gastroenterology* 140: 242–253, 2011. doi:10. 1053/i.gastro.2010.09.043.
- MohanKumar K, Kaza N, Jagadeeswaran R, Garzon SA, Bansal A, Kurundkar AR, Namachivayam K, Remon JI, Bandepalli CR, Feng X, Weitkamp JH, Maheshwari A. Gut mucosal injury in neonates is marked by macrophage infiltration in contrast to pleomorphic infiltrates in adult: evidence from an animal model. Am J Physiol Gastrointest Liver Physiol 303: G93–G102, 2012. doi:10.1152/ajpgi. 00016 2012
- Weitkamp J-H, Koyama T, Rock MT, Correa H, Goettel JA, Matta P, Oswald-Richter K, Rosen MJ, Engelhardt BG, Moore DJ, Polk DB. Necrotising enterocolitis is characterised by disrupted immune regulation and diminished mucosal regulatory (FOXP3)/ effector (CD4, CD8) T cell ratios. Gut 62: 73–82, 2013. doi:10.1136/ gutjnl-2011-301551.
- Akira S, Takeda K, Kaisho T. Toll-like receptors: critical proteins linking innate and acquired immunity. *Nat Immunol* 2: 675–680, 2001. doi:10.1038/90609.
- Neal MD, Sodhi CP, Jia H, Dyer M, Egan CE, Yazji I, Good M, Afrazi A, Marino R, Slagle D, Ma C, Branca MF, Prindle T Jr, Grant Z, Ozolek J, Hackam DJ. Toll-like receptor 4 is expressed on intestinal stem cells and regulates their proliferation and apoptosis via the p53 up-regulated modulator of apoptosis. J Biol Chem 287: 37296– 37308, 2012. doi:10.1074/jbc.M112.375881.
- Sato T, van Es JH, Snippert HJ, Stange DE, Vries RG, van den Born M, Barker N, Shroyer NF, van de Wetering M, Clevers H. Paneth cells constitute the niche for Lgr5 stem cells in intestinal crypts. Nature 469: 415–418, 2011. doi:10.1038/nature09637.
- Vaishnava S, Behrendt CL, Ismail AS, Eckmann L, Hooper LV. Paneth cells directly sense gut commensals and maintain homeostasis at the intestinal host-microbial interface. *Proc Natl Acad Sci USA* 105: 20858–20863, 2008. doi:10.1073/pnas.0808723105.
- McElroy SJ, Underwood MA, Sherman MP. Paneth cells and necrotizing enterocolitis: a novel hypothesis for disease pathogenesis. Neonatology 103: 10–20, 2013. doi:10.1159/000342340.
- Schaart MW, de Bruijn AC, Bouwman DM, de Krijger RR, van Goudoever JB, Tibboel D, Renes IB. Epithelial functions of the residual bowel after surgery for necrotising enterocolitis in human infants. J Pediatr Gastroenterol Nutr 49: 31–41, 2009. doi:10.1097/MPG. 0b013e318186d341.
- Zhang C, Sherman MP, Prince LS, Bader D, Weitkamp JH, Slaughter JC, McElroy SJ. Paneth cell ablation in the presence of Klebsiella pneumoniae induces necrotizing enterocolitis (NEC)-like injury in the small intestine of immature mice. *Dis Model Mech* 5: 522–532, 2012. doi:10.1242/dmm.009001.
- 15. Good M, Sodhi CP, Egan CE, Afrazi A, Jia H, Yamaguchi Y, Lu P, Branca MF, Ma C, Prindle T Jr, Mielo S, Pompa A, Hodzic Z, Ozolek JA, Hackam DJ. Breast milk protects against the development of necrotizing enterocolitis through inhibition of Toll-like receptor 4 in the intestinal epithelium via activation of the epidermal growth factor receptor. Mucosal Immunol 8: 1166–1179, 2015. doi:10.1038/mij.2015.30
- Ip S, Chung M, Raman G, Chew P, Magula N, DeVine D, Trikalinos T, Lau J. Breastfeeding and maternal and infant health outcomes in developed countries. Evid Rep Technol Assess (Full Rep)153: 1–186, 2007. doi:10.1542/gr.18-2-15.

- 17. Sullivan S, Schanler RJ, Kim JH, Patel AL, Trawoger R, Kiechl-Kohlendorfer U, Chan GM, Blanco CL, Abrams S, Cotten CM, Laroia N, Ehrenkranz RA, Dudell G, Cristofalo EA, Meier P, Lee ML, Rechtman DJ, Lucas A. An exclusively human milk-based diet is associated with a lower rate of necrotizing enterocolitis than a diet of human milk and bovine milk-based products. J Pediatr 156: 562–567.e1, 2010. doi:10.1016/j.jpeds.2009.10.040.
- Good M, Siggers RH, Sodhi CP, Afrazi A, Alkhudari F, Egan CE, Neal MD, Yazji I, Jia H, Lin J, Branca MF, Ma C, Prindle T, Grant Z, Shah S, Slagle D 2nd, Paredes J, Ozolek J, Gittes GK, Hackam DJ. Amniotic fluid inhibits Toll-like receptor 4 signaling in the fetal and neonatal intestinal epithelium. Proc Natl Acad Sci USA 109: 11330– 11335, 2012. doi:10.1073/pnas.1200856109.
- Gurien LA, Stallings-Archer K, Smith SD. Probiotic Lactococcus lactis decreases incidence and severity of necrotizing enterocolitis in a preterm animal model. J Neonatal Perinatal Med 11: 65–69, 2018. doi:10.3233/NPM-181740.
- Morgan RL, Preidis GA, Kashyap PC, Weizman AV, Sadeghirad B, Chang Y, Florez ID, Foroutan F, Shahid S, Zeraatkar D; McMaster Probiotic, Probiotic, and Synbiotic Work Group. Probiotics reduce mortality and morbidity in preterm, low-birth-weight infants: a systematic review and network meta-analysis of randomized trials. Gastroenterology 159: 467–480, 2020. doi:10.1053/j.gastro.2020. 05.096.
- Radulescu A, Zorko NA, Yu X, Besner GE. Preclinical neonatal rat studies of heparin-binding EGF-like growth factor in protection of the intestines from necrotizing enterocolitis. *Pediatr Res* 65: 437– 442, 2009. doi:10.1203/PDR.0b013e3181994fa0.
- Moorefield EC, McKee EE, Solchaga L, Orlando G, Yoo JJ, Walker S, Furth ME, Bishop CE. Cloned, CD117 selected human amniotic fluid stem cells are capable of modulating the immune response. PLoS One 6: e26535, 2011. doi:10.1371/journal.pone.0026535.
- Peak TC, Praharaj PP, Panigrahi GK, Doyle M, Su Y, Schlaepfer IR, Singh R, Vander Griend DJ, Alickson J, Hemal A, Atala A, Deep G. Exosomes secreted by placental stem cells selectively inhibit growth of aggressive prostate cancer cells. *Biochem Biophys Res Commun* 499: 1004–1010, 2018. doi:10.1016/j.bbrc.2018.04.038.
- Weil BR, Markel TA, Herrmann JL, Abarbanell AM, Meldrum DR. Mesenchymal stem cells enhance the viability and proliferation of human fetal intestinal epithelial cells following hypoxic injury via paracrine mechanisms. Surgery 146: 190–197, 2009. doi:10.1016/j. surq.2009.03.031.
- 25. Zani A, Cananzi M, Fascetti-Leon F, Lauriti G, Smith VV, Bollini S, Ghionzoli M, D'Arrigo A, Pozzobon M, Piccoli M, Hicks A, Wells J, Siow B, Sebire NJ, Bishop C, Leon A, Atala A, Lythgoe MF, Pierro A, Eaton S, De Coppi P. Amniotic fluid stem cells improve survival and enhance repair of damaged intestine in necrotising enterocolitis via a COX-2 dependent mechanism. Gut 63: 300–309, 2014. doi:10.1136/autinl-2012-303735.
- Drucker NA, McCulloh CJ, Li B, Pierro A, Besner GE, Markel TA. Stem cell therapy in necrotizing enterocolitis: current state and future directions. Semin Pediatr Surg 27: 57–64, 2018. doi:10.1053/j. sempedsurg.2017.11.011.
- McCulloh CJ, Olson JK, Zhou Y, Wang Y, Besner GE. Stem cells and necrotizing enterocolitis: a direct comparison of the efficacy of multiple types of stem cells. J Pediatr Surg 52: 999–1005, 2017. doi:10.1016/j.jpedsurg.2017.03.028.
- McCulloh CJ, Olson JK, Wang Y, Zhou Y, Tengberg NH, Deshpande S, Besner GE. Treatment of experimental necrotizing enterocolitis with stem cell-derived exosomes. *J Pediatr Surg* 53: 1215–1220, 2018. doi:10.1016/j.jpedsurg.2018.02.086.
- Matz EL, Thakker PU, Gu X, Terlecki RP, Dou L, Walker SJ, Lue T, Lin G, Atala A, Yoo JJ, Zhang Y, Jackson JD. Administration of secretome from human placental stem cell-conditioned media improves recovery of erectile function in the pelvic neurovascular injury model. J Tissue Eng Regen Med 14: 1394–1402, 2020. doi:10. 1002/term.3105.
- Mareschi K, Castiglia S, Sanavio F, Rustichelli D, Muraro M, Defedele D, Bergallo M, Fagioli F. Immunoregulatory effects on T lymphocytes by human mesenchymal stromal cells isolated from bone marrow, amniotic fluid, and placenta. *Exp Hematol* 44: 138– 150.e1, 2016. doi:10.1016/j.exphem.2015.10.009.
- Bergmann KR, Liu SX, Tian R, Kushnir A, Turner JR, Li HL, Chou PM, Weber CR, De Plaen IG. Bifidobacteria stabilize claudins at tight

- junctions and prevent intestinal barrier dysfunction in mouse necrotizing enterocolitis. Am J Pathol 182: 1595-1606, 2013. doi:10.1016/j. aipath.2013.01.013.
- Rentea RM, Welak SR, Fredrich K, Donohoe D, Pritchard KA, Oldham KT, Gourlay DM, Liedel JL. Early enteral stressors in newborns increase inflammatory cytokine expression in a neonatal necrotizing enterocolitis rat model. Eur J Pediatr Surg 23: 39-47, 2013. doi:10.1055/s-0032-1329704.
- Zani A, Cordischi L, Cananzi M, De Coppi P, Smith VV, Eaton S, Pierro A. Assessment of a neonatal rat model of necrotizing enterocolitis. Eur J Pediatr Surg 18: 423-426, 2008. doi:10.1055/s-2008-1038951
- De Coppi P, Bartsch G Jr, Siddigui MM, Xu T, Santos CC, Perin L, Mostoslavsky G, Serre AC, Snyder EY, Yoo JJ, Furth ME, Soker S, Atala A. Isolation of amniotic stem cell lines with potential for therapy. Nat Biotechnol 25: 100-106, 2007. doi:10.1038/nbt1274.
- Barlow B, Santulli TV, Heird WC, Pitt J, Blanc WA, Schullinger JN. An experimental study of acute neonatal enterocolitis-the importance of breast milk. J Pediatr Surg 9: 587-595, 1974. doi:10.1016/ 0022-3468(74)90093-1.
- Dou L, Matz EL, Gu X, Shu F, Paxton J, Song J, Yoo J, Atala A, Jackson J, Zhang Y. Non-invasive cell tracking with brighter and red-transferred Luciferase for potential application in stem cell therapy. Cell Transplant 28: 1542-1551, 2019. doi:10.1177/09636897 19885078
- Tu S-H, Hsieh Y-C, Huang L-C, Lin C-Y, Hsu K-W, Hsieh W-S, Chi W-M, Lee C-2864H. A rapid and quantitative method to detect human circulating tumor cells in a preclinical animal model. BMC Cancer 17: 440, 2017. doi:10.1186/s12885-017-3419-x.
- Maurer CR, Qi R, Raghavan V. A linear time algorithm for computing exact Euclidean distance transforms of binary images in arbitrary dimensions. IEEE Trans Pattern Anal Mach Intell 25: 265-270, 2003. doi:10.1109/TPAMI.2003.1177156.
- Weis VG, Sousa JF, LaFleur BJ, Nam KT, Weis JA, Finke PE, Ameen NA, Fox JG, Goldenring JR. Heterogeneity in mouse spasmolytic polypeptide-expressing metaplasia lineages identifies markers of metaplastic progression. Gut 62: 1270-1279, 2013. doi: 10.1136/gutjnl-2012-302401.
- Weis VG, Petersen CP, Weis JA, Meyer AR, Choi E, Mills JC, Goldenring JR. Maturity and age influence chief cell ability to transdifferentiate into metaplasia. Am J Physiol Gastrointest Liver Physiol 312: G67-G76, 2017. doi:10.1152/ajpgi.00326.2016.
- Goncalves FLL, Gallindo RM, Soares LMM, Figueira RL, Volpe FAP, Pereira-da-Silva MA, Sbragia L. Validation of protocol of experimental necrotizing enterocolitis in rats and the pitfalls during the procedure. Acta Cir Bras 28: 19-25, 2013. doi:10.1590/S0102-8650201
- van der Flier LG, Haegebarth A, Stange DE, van de Wetering M, Clevers H. OLFM4 is a robust marker for stem cells in human intestine and marks a subset of colorectal cancer cells. Gastroenterology 137: 15-17, 2009. doi:10.1053/j.gastro.2009.05.035.
- Formeister EJ, Sionas AL, Lorance DK, Barkley CL, Lee GH, Magness ST. Distinct SOX9 levels differentially mark stem/progenitor populations and enteroendocrine cells of the small intestine epithelium. Am J Physiol Gastrointest Liver Physiol 296: G1108-G1118, 2009. doi:10.1152/ajpgi.00004.2009.
- Roche KC, Gracz AD, Liu XF, Newton V, Akiyama H, Magness ST. SOX9 maintains reserve stem cells and preserves radioresistance in mouse small intestine. Gastroenterology 149: 1553-1563.e10, 2015. doi:10.1053/i.gastro.2015.07.004.
- Bastide P, Darido C, Pannequin J, Kist R, Robine S, Marty-Double C, Bibeau F, Scherer G, Joubert D, Hollande F, Blache P, Jay P. Sox9 regulates cell proliferation and is required for Paneth cell differentiation in the intestinal epithelium. J Cell Biol 178: 635-648, 2007. doi:10.1083/jcb.200704152.
- Farin HF, Van Es JH, Clevers H. Redundant sources of Wnt regulate intestinal stem cells and promote formation of Paneth cells. Gastroenterology 143: 1518-1529.e7, 2012. doi:10.1053/j.gastro. 2012.08.031.
- Patel RM, Underwood MA. Probiotics and necrotizing enterocolitis. Semin Pediatr Surg 27: 39-46, 2018. doi:10.1053/j.sempedsurg.
- Fischer UM, Harting MT, Jimenez F, Monzon-Posadas WO, Xue H, Savitz SI, Laine GA, Cox CS Jr. Pulmonary passage is a major

- obstacle for intravenous stem cell delivery: the pulmonary first-pass effect. Stem Cells Dev 18: 683-692, 2009. doi:10.1089/ scd.2008.0253.
- Yang J, Watkins D, Chen CL, Zhang HY, Zhou Y, Velten M, Besner **GE.** A technique for systemic mesenchymal stem cell transplantation in newborn rat pups. J Invest Surg 25: 405-414, 2012. doi:10.3109/ 08941939 2012 661519
- Ghionzoli M, Cananzi M, Zani A, Rossi CA, Leon FF, Pierro A, Eaton S, De Coppi P. Amniotic fluid stem cell migration after intraperitoneal injection in pup rats: implication for therapy. Pediatr Surg Int 26: 79-84, 2010. doi:10.1007/s00383-009-2504-x.
- Wang M, Liang C, Hu H, Zhou L, Xu B, Wang X, Han Y, Nie Y, Jia S, Liang J, Wu K. Intraperitoneal injection (IP), Intravenous injection (IV) or anal injection (AI)? Best way for mesenchymal stem cells transplantation for colitis. Sci Rep 6: 30696, 2016. doi:10.1038/srep 30696
- Yang J, Watkins D, Chen C-L, Bhushan B, Zhou Y, Besner GE. Heparin-binding epidermal growth factor-like growth factor and mesenchymal stem cells act synergistically to prevent experimental necrotizing enterocolitis. J Am Coll Surg 215: 534-545, 2012. doi:10.1016/j.jamcollsurg.2012.05.037.
- Zani A, Cananzi M, Lauriti G, Fascetti-Leon F, Wells J, Siow B, Lythgoe MF, Pierro A, Eaton S, De Coppi P. Amniotic fluid stem cells prevent development of ascites in a neonatal rat model of necrotizing enterocolitis. Eur J Pediatr Surg 24: 057-060, 2013. doi:10.1055/s-0033-1350059.
- Criss CN, Selewski DT, Sunkara B, Gish JS, Hsieh L, McLeod JS, Robertson JO, Matusko N, Gadepalli SK. Acute kidney injury in necrotizing enterocolitis predicts mortality. Pediatr Nephrol 33: 503-510, 2018. doi:10.1007/s00467-017-3809-y.
- Halpern MD, Holubec H, Dominguez JA, Meza YG, Williams CS, Ruth MC, McCuskey RS, Dvorak B. Hepatic inflammatory mediators contribute to intestinal damage in necrotizing enterocolitis. Am J Physiol Gastrointest Liver Physiol 284: G695-G702, 2003. doi:10.1152/ajpgi.00353.2002.
- Nino DF, Zhou Q, Yamaguchi Y, Martin LY, Wang S, Fulton WB, Jia H, Lu P, Prindle T, Jr, Zhang F, Crawford J, Hou Z, Mori S, Chen LL, Guajardo A, Fatemi A, Pletnikov M, Kannan RM, Kannan S, Sodhi CP, Hackam DJ. Cognitive impairments induced by necrotizing enterocolitis can be prevented by inhibiting microglial activation in mouse brain. Sci Transl Med 10: eaan0237, 2018. doi:10.1126/ scitranslmed.aan0237.
- Ellsbury DL, Clark RH, Ursprung R, Handler DL, Dodd ED, Spitzer AR. A multifaceted approach to improving outcomes in the NICU: the Pediatrix 100 000 Babies Campaign. Pediatrics 137: e20150389, 2016. doi:10.1542/peds.2015-0389.
- Fitzgibbons SC, Ching Y, Yu D, Carpenter J, Kenny M, Weldon C, Lillehei C, Valim C, Horbar JD, Jaksic T. Mortality of necrotizing enterocolitis expressed by birth weight categories. J Pediatr Sura 44: 1072-1075, 2009. doi:10.1016/j.jpedsurg.2009.02.013.
- Fredriksson F, Engstrand Lilja H. Survival rates for surgically treated necrotising enterocolitis have improved over the last four decades. Acta Paediatr 108: 1603-1608, 2019. doi:10.1111/apa.14770.
- Duro D, Kalish LA, Johnston P, Jaksic T, McCarthy M, Martin C, Dunn JC, Brandt M, Nobuhara KK, Sylvester KG, Moss RL, Duggan C. Risk factors for intestinal failure in infants with necrotizing enterocolitis: a Glaser Pediatric Research Network study. J Pediatr 157: 203-208.e1, 2010. doi:10.1016/j.jpeds.2010.02.023.
- Elfvin A, Dinsdale E, Wales PW, Moore AM. Low birthweight, gestational age, need for surgical intervention and gram-negative bacteraemia predict intestinal failure following necrotising enterocolitis. Acta Paediatr 104: 771-776, 2015. doi:10.1111/apa.12997.
- Hintz SR, Kendrick DE, Stoll BJ, Vohr BR, Fanaroff AA, Donovan EF, Poole WK, Blakely ML, Wright L, Higgins R; NICHD Neonatal Research Network. Neurodevelopmental and growth outcomes of extremely low birth weight infants after necrotizing enterocolitis. Pediatrics 115: 696-703, 2005. doi:10.1542/peds.2004-0569.
- Rees CM, Pierro A, Eaton S. Neurodevelopmental outcomes of neonates with medically and surgically treated necrotizing enterocolitis. Arch Dis Child Fetal Neonatal Ed 92: F193-F198, 2007. doi:10.1136/ adc.2006.099929.
- D'Antiga L, Goulet O. Intestinal failure in children: the European view. J Pediatr Gastroenterol Nutr 56: 118-126, 2013. doi:10.1097/ mpg.0b013e318268a9e3.

- Dibaise JK, Young RJ, Vanderhoof JA. Enteric microbial flora, bacterial overgrowth, and short-bowel syndrome. Clin Gastroenterol Hepatol 4: 11-20, 2006. doi:10.1016/j.cgh.2005.10.020.
- Hukkinen M, Mutanen A, Pakarinen MP. Small bowel dilation in children with short bowel syndrome is associated with mucosal damage, bowel-derived bloodstream infections, and hepatic injury. Surgery 162: 670-679, 2017. doi:10.1016/j.surg.2017.04.018.
- Tayman C, Aydemir S, Yakut I, Serkant U, Ciftci A, Arslan E, Koc O. TNF-α blockade efficiently reduced severe intestinal damage in necrotizing enterocolitis. J Invest Surg 29: 209-217, 2016. doi:10.3109/08941939.2015.1127449.
- Esteve-Sole A, Deya-Martinez A, Teixido I, Ricart E, Gompertz M, Torradeflot M, de Moner N, Gonzalez EA, Plaza-Martin AM, Yague J, Juan M, Alsina L. Immunological changes in blood of newborns exposed to anti-TNF- α during pregnancy. Front Immunol 8: 1123, 2017. doi:10.3389/fimmu.2017.01123.
- Khoury O, Atala A, Murphy SV. Stromal cells from perinatal and adult sources modulate the inflammatory immune response in vitro by decreasing Th1 cell proliferation and cytokine secretion. Stem Cells Transl Med 9: 61-73, 2020. doi:10.1002/sctm.19-0123.
- Silini AR, Magatti M, Cargnoni A, Parolini O. Is immune modulation the mechanism underlying the beneficial effects of amniotic cells and their derivatives in regenerative medicine? Cell Transplant 26: 531-539, 2017. doi:10.3727/096368916X693699.
- Guan Y-T, Xie Y, Li D-S, Zhu Y-Y, Zhang X-L, Feng Y-L, Chen Y-P, Xu L-J, Liao P-F, Wang G. Comparison of biological characteristics of mesenchymal stem cells derived from the human umbilical cord and decidua parietalis. Mol Med Rep 20: 633-639, 2019. doi: 10.3892/mmr.2019.10286.
- Kong P, Xie X, Li F, Liu Y, Lu Y. Placenta mesenchymal stem cell accelerates wound healing by enhancing angiogenesis in diabetic Goto-Kakizaki (GK) rats. Biochem Biophys Res Commun 438: 410-419, 2013. doi:10.1016/j.bbrc.2013.07.088.
- Baregamian N, Song J, Bailey CE, Papaconstantinou J, Evers BM, **Chung DH.** Tumor necrosis factor-α and apoptosis signal-regulating kinase 1 control reactive oxygen species release, mitochondrial autophagy, and c-Jun N-terminal kinase/p38 phosphorylation during necrotizing enterocolitis. Oxid Med Cell Longev 2: 297-306, 2009. doi:10.4161/oxim.2.5.9541.
- Seitz G, Warmann SW, Guglielmetti A, Heitmann H, Ruck P, Kreis ME, Fuchs J. Protective effect of tumor necrosis factor alpha antibody on experimental necrotizing enterocolitis in the rat. J Pediatr Surg 40: 1440-1445, 2005. doi:10.1016/j.jpedsurg.2005.05.043.
- Yu R, Jiang S, Tao Y, Li P, Yin J, Zhou Q. Inhibition of HMGB1 improves necrotizing enterocolitis by inhibiting NLRP3 via TLR4 and NF-κB signaling pathways. J Cell Physiol 234: 13431–13438, 2019. doi:10.1002/jcp.28022.
- Nino DF, Sodhi CP, Egan CE, Zhou Q, Lin J, Lu P, Yamaguchi Y, Jia H, Martin LY, Good M, Fulton WB, Prindle T Jr, Ozolek JA, Hackam DJ. Retinoic acid improves incidence and severity of necrotizing

- enterocolitis by lymphocyte balance restitution and repopulation of LGR5+ intestinal stem cells. Shock 47: 22-32, 2017. doi:10.1097/ SHK.0000000000000713.
- Li B, Lee C, Cadete M, Zhu H, Koike Y, Hock A, Wu RY, Botts SR, Minich A, Alganabi M, Chi L, Zani-Ruttenstock E, Miyake H, Chen Y, Mutanen A, Ngan B, Johnson-Henry KC, De Coppi P, Eaton S, Maattanen P, Delgado-Olguin P, Sherman PM, Zani A, Pierro A. Impaired Wnt/β-catenin pathway leads to dysfunction of intestinal regeneration during necrotizing enterocolitis. Cell Death Dis 10: 743, 2019. doi:10.1038/s41419-019-1987-1.
- Li B, Lee C, O'Connell JS, Antounians L, Ganji N, Alganabi M, Cadete M, Nascimben F, Koike Y, Hock A, Botts SR, Wu RY, Miyake H, Minich A, Maalouf MF, Zani-Ruttenstock E, Chen Y, Johnson-Henry KC, De Coppi P, Eaton S, Maattanen P, Delgado Olguin P, Zani A, Sherman PM, Pierro A. Activation of Wnt signaling by amniotic fluid stem cell-derived extracellular vesicles attenuates intestinal injury in experimental necrotizing enterocolitis. Cell Death Dis 11: 750, 2020. doi:10.1038/s41419-020-02964-2.
- Blache P, van de Wetering M, Duluc I, Domon C, Berta P, Freund JN, Clevers H, Jay P. SOX9 is an intestine crypt transcription factor, is regulated by the Wnt pathway, and represses the CDX2 and MUC2 genes. J Cell Biol 166: 37-47, 2004. doi:10.1083/jcb.2003
- Miyoshi H, VanDussen KL, Malvin NP, Ryu SH, Wang Y, Sonnek NM, Lai CW, Stappenbeck TS. Prostaglandin E2 promotes intestinal repair through an adaptive cellular response of the epithelium. EMBO J 36: 5-24, 2017. doi:10.15252/embj.201694660.
- Higginbotham JN, Zhang Q, Jeppesen DK, Scott AM, Manning HC, Ochieng J, Franklin JL, Coffey RJ. Identification and characterization of EGF receptor in individual exosomes by fluorescence-activated vesicle sorting. J Extracell Vesicles 5: 29254, 2016. doi:10.3402/jev.v5.29254.
- Zhang H, Deng T, Liu R, Bai M, Zhou L, Wang X, Li S, Wang X, Yang H, Li J, Ning T, Huang D, Li H, Zhang L, Ying G, Ba Y. Exosome-delivered EGFR regulates liver microenvironment to promote gastric cancer liver metastasis. Nat Commun 8: 15016, 2017. doi:10.1038/ncomms15016.
- Ahn SY, Chang YS, Kim JH, Sung SI, Park WS. Two-year follow-up outcomes of premature infants enrolled in the phase I trial of mesenchymal stem cells transplantation for bronchopulmonary dysplasia. J Pediatr 185: 49-54.e2, 2017. doi:10.1016/j.jpeds.2017.02.061.
- Ahn SY, Chang YS, Sung SI, Park WS. Mesenchymal stem cells for severe intraventricular hemorrhage in preterm infants: phase I doseescalation clinical trial. Stem Cells Transl Med 7: 847-856, 2018. doi:10.1002/sctm.17-0219.
- Chang YS, Ahn SY, Yoo HS, Sung SI, Choi SJ, Oh WI, Park WS. Mesenchymal stem cells for bronchopulmonary dysplasia: phase 1 dose-escalation clinical trial. J Pediatr 164: 966-972.e6, 2014. doi: 10.1016/j.jpeds.2013.12.011.